2014

Characterization of Hybrid Electronic Materials Using Atomic Force Microscopy

Madhavi Divakar Rajathadripura
Louisiana State University and Agricultural and Mechanical College

CHARACTERIZATION OF HYBRID ELECTRONIC MATERIALS USING ATOMIC FORCE MICROSCOPY

A Thesis

Submitted to the Graduate Faculty of the
Louisiana State University and
Agricultural and Mechanical College
in partial fulfillment of the
requirements for the degree of
Master of Science

in

The Department of Electrical and Computer Engineering

by
Madhavi Divakar Rajathadripura
B.E., Visvesvaraya Technological University, 2008
August 2014

Dedicated to my husband Sunada Chakravarthy and to my parents Divakar and Gayathri

ACKNOWLEDGEMENTS

First, I would like to thank my graduate advisor Dr. Theda Daniels-Race for giving me an opportunity to work with her. Without her guidance and encouragement this work would have been impossible. I would also like to acknowledge my committee members Dr. Martin Feldman and Dr. Georgios Veronis for taking time off from their busy schedules to provide valuable suggestions. I would also like to express my gratitude to Dr. Warner, and his research group at LSU chemistry department for providing us with the samples for this project. I am thankful to my lab mates Kalyan Kanakamedala, Dr. Anirban Sarkar, Hao Wang, and Shubodip Maulik for all the technical discussions that helped me in completing this work.

I would also like to thank Louisiana Board of Regents (LEQSF(2011-14)-RD-A-07), NASA (2011)-DART-44, Dr. Kristina Johnson, and the AES Corporation for providing financial support for my Master's research work. Finally, I would like to thank my family and friends who have always supported me with unconditional love.

TABLE OF CONTENTS

LIST OF FIGURES

ABSTRACT

Miniaturization in the electronics industry has been driven by advancements in material science. Recently, Hybrid Electronic Materials (HEMs) have been postulated to have unique material properties that can be used within the semiconductor industry. As such, the main focus of this research is to characterize the relevant properties of HEMs using atomic force microscopy (AFM), conductive probe atomic force microscopy (CP-AFM), and Raman spectroscopy techniques. Emphasis is placed on characterizing [R6G][TPB] GUMBOS which are a Group of Uniform Materials Based on Organic Salts. GUMBOS exhibit properties such as fluorescence and magnetic susceptibility, both of which may be important with respect to their applications within the electronics industry.

Next, the functionalization of substrates as HEM templates for nanoscale device technologies is an area of both scientific interest and technological necessity. Historically, Aminopropyltriethoxy Silane (APTES) has been used as an effective silane (SiH_4) coupling agent to enhance adhesion. In this work, a study of the morphology of APTES on silicon substrates, using both AFM and Raman spectroscopy has been undertaken.

Finally, a great deal of research has focused on characterizing the mechanical and chemical properties of biocompatible and biodegradable materials. Therefore, the last part of this work focuses on characterizing the morphology of zein fibers. Zein is a class of biopolymer which falls into the category of prolamine proteins of corn (maize). Although not specifically identified as an electronic material by itself, zein has proven to be a valuable component of composite (hybrid) materials exhibiting characteristics of high tensile strength, selective permeability, and resistance to microbial attack, to name a few. If amenable to inte-

gration with sensor or biomedical electronics, investigating the processing mechanics of zein may be invaluable to potential device applications. Thus, this research takes a step in the direction of understanding the deposition mechanics and morphology of zein on substrates, using the technique of electrospraying, in conjunction with AFM, scanning electron microscopy (SEM), and Raman spectroscopy.

1. INTRODUCTION

1.1 Background and Overview

Nanotechnology refers to the study and manipulation of matter in the atomic or molecular scale. Norio Taniguchi first coined the term in the year 1974 [1]. The era of nanotechnology began in the year 1959, when Richard Feynman mentioned in his speech, "there's plenty of room at the bottom" [2]. Nanotechnology incorporates length scales between 1 to 100nm. From the perspective of solid state electronics, device fabrication can be accomplished by a "top-down" or "bottom-up" approach. The top-down approach involves the use of now traditional tools of semiconductor device fabrication (i.e. – E-beam lithography, focused ion beam systems or FIBs) and methods of fabrication of effectively "machining" a structure down to the nanoscale. The bottom-up processes take on the task of creating conditions whereby atoms or molecules either self-assemble or may be manipulated into formations that exhibit the desired nanoscale electronic structure or device behavior [3,4]. These approaches have led to the invention of a class of materials known as *hybrid electronic materials* or HEMs.

HEMs are combinations of organic and inorganic materials and as innovative advanced materials, have potential applications in numerous fields namely, electronics, optics, mechanics, and biology [5]. The concept of inorganic and organic composites takes on a new dimension as we move towards nanocomposite materials, where interactions of components take place on a molecular level. According to Judeinstein and Sanchez these materials can be classified into two groups [5]. In *Class I* materials, organic and inorganic materials exchange weak interactions with weak bonds (hydrogen or Van der Waals bonds); these weak bonds

form during collisions to form whole structures. In *class II materials*, organic and inorganic materials are linked together through strong chemical bonds such as covalent or ionic bonds. The types of bonds involved in these two materials (organic and inorganic) are different, and they exhibit different behavior when the size of these materials change from bulk to nanometer sized objects. This change in size affects the properties of nanophased materials, which leads to changes in mechanical properties, electronic properties, and thermal properties [5]. Organic polymers have high flexibility, good film forming capability, and the ability to design functional groups; whereas inorganic compounds possess great tensile strength, good gas barrier properties, and high mechanical tensile stabilities. Alternating layers of organic and inorganic materials can be bound together due to their adhesive properties. The traditional methods used to characterize these organic-inorganic materials include chromatography, light and x-ray scattering, x-ray diffraction, and other optical techniques. In turn some spectroscopy techniques used are fluorescence, IR (infrared), UV-VIS (ultraviolet-visible), mass spectroscopy, and X-ray spectroscopy.

Given the unique forms of hybrid electronic materials investigated in this work, in this thesis we characterize different types of HEMs using Atomic Force Microscopy (AFM), Conductive Probe Atomic Force Microscopy (CP-AFM), and Raman spectroscopy. As it is our long-term goal to discover combinations of HEMs for uses ranging from light emitting diodes and field effect transistors to sensors and solar cells, this study is a step toward future micro and nano-electronic device development.

1.2 Literature Review

This section provides a brief overview of experiments that have been carried out to characterize different hybrid materials. Hybrid materials, which are combinations of organic

and in-organic materials can be prepared by various techniques. In this section, hybrid materials prepared using sol-gel techniques, ionic liquids, and bionanocomposites are discussed.

The sol-gel technique using metal alkoxides is one of the most widely used techniques to prepare hybrid materials as described by Ogoshi and Chujo [6] . These hybrid materials as obtained from sol-gel techniques have applications in electronics, optics, sensors, mechanics, membranes, and optics [6]. Nivens et.al have investigated the usage of sol-gels for fiber optic sensors application. In their study, sol-gel was prepared by co-polymerizing both PDMS (Polydimethylsiloxane) and organo-silane coupling agents, such as GPTMS (Glycidoxypropyltriethoxysilane) and APTES (Aminopropyltriethoxysilane), with TEOS (Tetraethylorthosilicate) [7]. For our study, we have prepared 3-Aminopropyl triethoxysilane (APTES) using the sol-gel process where a thin layer of APTES is deposited on a silicon substrate. Weimer et al. have evaluated electronic properties of sol-gel derived oxide films on silicon substrates [8]. Oxides (SiO_2, $Al2O_3$, B_2O_3, BaO) were deposited by spinning polymermized metal alkoxide [8]. Oxides obtained due to sol-gel processing are of enormous interest due to their simple formation, low cost, and reduced annealing time[9]. Weimer et al. have demonstrated some sol-gel derived oxides on silicon displays of low interface state density which have proved to be very good insulators and useful in MOSFET applications [8]. Warren et al. also studied the physical and electronic properties of sol-gel dielectric thin films on silicon substrates. They successfully fabricated sol-gel thin films on silicon substrates [9]. Recently Banger et al. have validated their study by deposition of amorphous metal oxide semiconducting thin films using a 'sol-gel on chip' which uses the 'built-in' chemical reactivity of transition metal alkoxide [10]. Their sol-gel process is carried out using a temperature-controlled hot plate in the presence of air. At a low annealing temperature of 230^0 C, the

device fabricated using sol-gel on chip has proven to have an excellent on-off ratio, low hysteresis, small sub threshold slopes, and high mobility [10]. Banger et al. have built high-performance solution-processed metal oxide thin-film transistors, which can be operated at low-temperature using a 'sol-gel on chip' process.

Another method of preparation of hybrid materials is by using ionic liquids. Ionic liquids belong to the family of molten salts but are different from conventional molten salts. The melting points of traditional ionic liquids are below 100^0 C and have good thermal stability, high ionic conductivity, and high synthetic flexibility [11]. Ionic liquids are used to prepare a broad range of materials, such as metal structures, non-metal elements, silicas, organosilicas, metal oxides, and ionic liquid-functionalized materials [11]. Ma et al. first reported synthesis of SiO_2 aerogel using an ionic liquid. The authors used 1-ethyl-3 methylimidazolium bis(trifluoromethylsulfonyl)imide ([EMim][NTf2]) as a solvent instead of water[12]. Notably, Nakashima and Kimizuka fabricated hollow TiO_2 microspheres at the interface between an ionic liquid and a toluene droplet [13]. Also, Zhou and Antonietti used ionic liquids to obtain spherical TiO_2 aggregates from TiO_2 nanoparticles [14]. More recently researchers have focused on using functionalized ionic liquids for the preparation and stabilization of metal nanoparticles as certain functional groups bind and stabilize metal nanoparticles efficiently [11]. Lee et al. have used different numbers of thiol groups to develop several thiol-functionalized ionic liquids, and they also prepared ionic liquid-protected Au, Pt, and Pd nanoparticles by reducing $HAuCl_4$, $Na_2\ Pt(OH)_6$, or $Na_2\ PdCl_4$ with NaBH4 [11, 15]

One form of ionic liquid based hybrid material (and upon which we have focused in this thesis) is known as GUMBOS or a **G**roup of **U**niform **M**aterials **B**ased on **O**rganic **S**alts. Discovered and introduced to the literature by Professor Isiah M. Warner (LSU, Department

of Chemistry) as a new class of micro and nanoparticles in 2008, [16] these were later given the moniker of GUMBOS [17]. These materials are essentially the "frozen" (solid-state) form ionic liquids that defy the historical 100^0 C or less melting point. The average size of GUMBOS based particles ranges from 14 to 198nm [18]. Prior to Warner's work, room temperature (~25^0C) ionic liquids (RTIL) had been used in applications involving nanosynthesis, chromatography, extraction, and catalysis [18-19]. However, GUMBOS have been reported to host a range of functionalities, be these in terms of size or structure (i.e.-nano particles, rods, or wires) [20] or properties such as fluorescence [21 17 22], magnetism [18], and anti-microbial effects [23] , to name a few. In this thesis, we investigated one form of GUMBOS based on Rhodamine 6G Tetraphenylborate or [R6G][TPB]. In addition to fluorescence, the Warner Group had noted that [R6G][TPB] exhibited high photostability, another desirable property for potential HEM optoelectronic applications.

Lastly, hybrid materials can also be synthesized using bionanocomposites. Hybrid materials synthesized using bionanocomposites have diverse applications. They are used in tissue engineering, biosensing devices, biocatalysts, and drug delivery systems[24]. Ariga et al. have summarized several important studies on composite materials between peptides (or amino acids) and mesoporous silicates [24,25]. As the usage of silica is beneficial to the stable immbobilization of proteins [24], Lee et al. used mesocellular mesoporous silica material for the immobilization of a-chymotrypsin [26]. Also, Lin and coworkers also reported in-vitro uptake and release profiles of cytochrome c by MCM-41 mesoporous silica nanoparticles [24]. Additionally, Bottcher et al. have discussed the use of inorganic supports to assemble microorganisms such as yeast cells, bacteria, and algae for biocatalysis and bioabsorption [27]. A novel clay hybrid for biosensor applications was developed by Zou and coworkers [28]. Bi-

opolymer-clay nanocomposites have potential applications in fertilizers, food additives, plastic fillers, fungicides, insecticides, molecular sieves, anti-microbials, and synthetic catalytic materials [24, 29]. Szabo et al. have performed systematic studies on adsorption of protamine and papain proteins on a saponite clay mineral [30]. Moreover, Forano et al. have worked on chitosan-clay nanocomposites that incorporate silver (Ag) nanoparticles or Ag-zeolites that can be prepared as films that show antimicrobial activity, which has application in food packaging industries [31].

Due to advancements in materials science relating to biodegradable and biocompatible materials, we have focused a part of this study on characterizing zein fibers, which is commonly known as corn protein. Based on its solubility in aqueous solution, zein was first identified in the year 1897 [32]. Croston et al.[33] published an article in 1945 which detailed different methodologies of zein preparation such as wet spinning and dry spinning. Additionally, the paper also discussed the properties of zein nanofibers and their uses in the textile industry. Although not identified as an *electronic* material per se, from a nanotechnological point of view, zein fibers have numerous applications. Zein, when reacted with organic compounds, forms a meshwork consisting of tubular structures which, in turn, is inert and microbiologically resistant [34]. In order to improve mechanical and thermal properties, controlling the uniformity and organization of zein films at the nanolevel is important [35]. Shi et al.[34c] tested different solvents and ascertained that a smoother and structurally more homogenous film is obtained from ethanol than when acetic acid is used. Results such as these may prove useful in terms of applications requiring the deposition of thin films. Whereas interest in the latter would typically tend towards nanoelectronics, in the case of our long-term research understanding the potential sensing capability of zein as a nanomaterial is a worthy

goal. For example, the aim of a biocompatible nanosensor may be to reduce the time for pathogen detection [34a]. When such a nanosensor is directly placed inside packaged materials it can serve as "electronic tongue" or "nose" by detecting chemicals released during food spoilage [34a, 36]. Conceivably, a zein-based nanosensor, designed in conjunction with HEMs-based components, could act as an ecologically and economically efficient overall nanoscale electronic detection system.

Finally, as may be noted from the above, HEMs span a wide range of materials and applications. This brief review of the literature, with respect to methods of sample preparation and related experimental work, is intended to serve as a both a guide to future study as well as the source of motivation for the work described in this thesis. In the sections that follow, we will present the details of and data obtained from a selected set of HEMs. As a body of original research, our work serves as yet another key step along the path to the realization of nanoscale phenomena that may be applied to the next-generation of device and circuit technologies.

1.3 Research Objectives

Research objectives of this thesis are as follows:

1. To characterize the morphology and electronic phenomena exhibited by organic-inorganic materials using Atomic Force Microscopy (AFM) and Conductive-Probe AFM.
2. To analyze HEM structures at a molecular scale by using Raman spectroscopy
3. To determine nanoscale properties of HEMs that may be exploited in the development of nanomolecular based devices.

2. EXPERIMENTAL TECHNIQUES

2.1 Atomic Force Microscopy

Atomic Force Microscopy (AFM) is one of the Scanning Probe Microscopy (SPM) based techniques. It was invented in 1986 by G. Binnig, C.F. Quate, and Ch. Gerber [37]. To measure the surface morphology and properties of a sample, AFM uses a sharp tip that is connected to a cantilever. The cantilever is bent in positive and negative directions depending on the attractive or repulsive forces exerted during the interaction between the tip and the sample. Figure 1 shows our AFM laboratory set-up.

In AFM a constant force is applied between the probe and a sample as the probe is raster scanned across the sample surface. A 3-dimensional image is constructed by monitoring the motion of the tip. Unlike Scanning Tunneling Microscopy (STM), AFM does not require a conducting surface to scan the sample surface. With this instrument insulators, organic materials, biological macromolecules, polymers, ceramics, and glasses can be imaged under different environmental conditions [4]. These basic principles of AFM have led to the invention of different microscopy techniques such as, Magnetic Force Microscopy (MFM), Frictional Force Microscopy (FFM), Dipping Force Microscopy (DFM), and Electrostatic Force Microscopy (EFM) [38].

2.2 AFM Components

Figure 2 shows block diagram of AFM components. Piezoelectric material, a force transducer, and a feedback controller are basic components of AFM. Piezoelectric materials are electromechanical transducers; they convert electrical potential to mechanical motion. These materials are used to control the motion of the probe as it scanned across the surface.

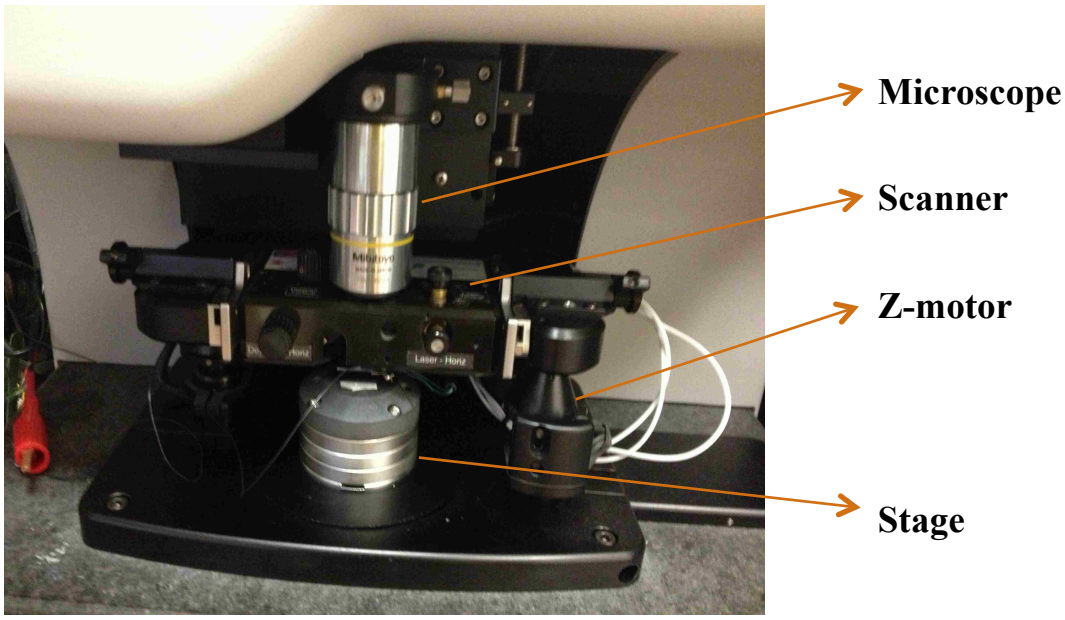

Figure 1: AFM laboratory set-up

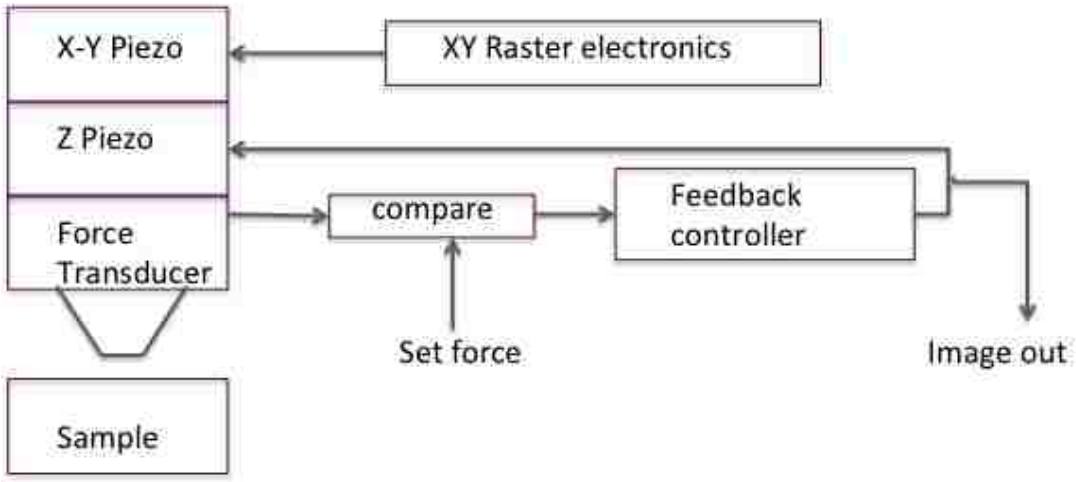

Figure 2: Block diagram of AFM components

The force between probe and surface is measured using force transducers. The voltage of the transducer varies when the probe comes into contact with the surface. The output of the transducer increases as the probe applies higher force on the sample.

Figure 3 illustrates a block diagram of a feedback loop. Feedback control maintains the force constant by controlling the expansion of the z-piezoelectric transducer. X-Y piezoelectric ceramics are used to scan the surface using a raster scanning pattern.

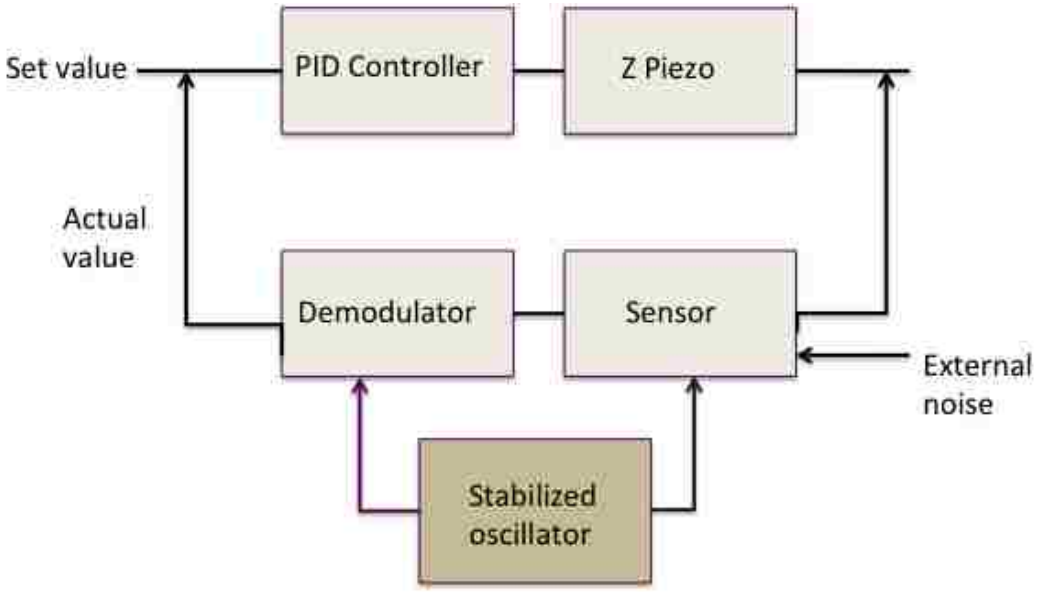

Figure 3: Block diagram of feedback loop

2.3 Modes of Operation

2.3.1 Contact mode

Figure 4 represents AFM operated in contact mode. In contact mode, the tip is brought closer to the sample surface. The tip mechanically contacts the sample surface with the application of force. As the tip moves closer to the surface, a repulsive force is generated between sample and tip. Contact mode is also known as variable deflection mode [38]. The cantilever used in contact mode is relatively soft with a spring constant (K_c) between 0.05 and 1.00 N/m. The magnitude of force applied on the sample by the cantilever is in the range of 10^{-7} to 10^{-6} N [39]. Sample damages are relatively high in this mode due to the large amount of lateral forces exerted on the sample surface.

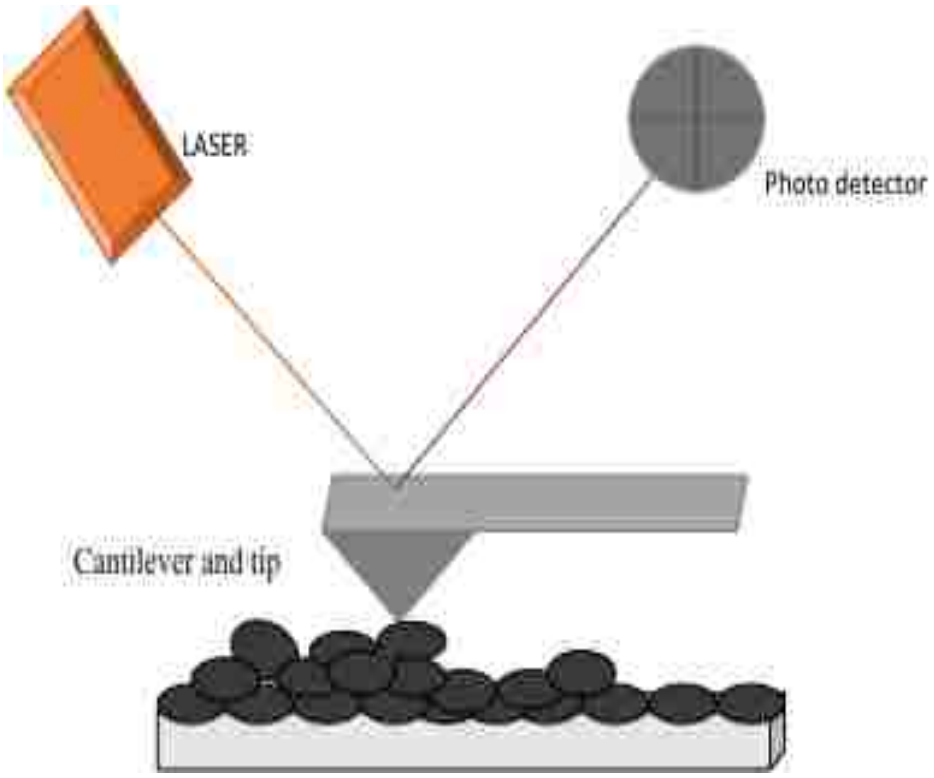

Figure 4: AFM in contact mode

Figure 5 represents the force versus distance curve of contact mode AFM. As the Van der Waals force becomes positive, the atoms are in contact. When atoms in the tip and the sample are brought together, and when the distance between them is large, they tend to attract to each other. However, when they are brought very close, the electron clouds of the tip and sample atoms begin to repel each other electrostatically. Electrostatic repulsion weakens the attractive force between atoms as the interatomic distance continuous to decrease. In addition to Van der Waals forces some of the other forces present in contact mode AFM are those exerted by the cantilever and capillary forces.

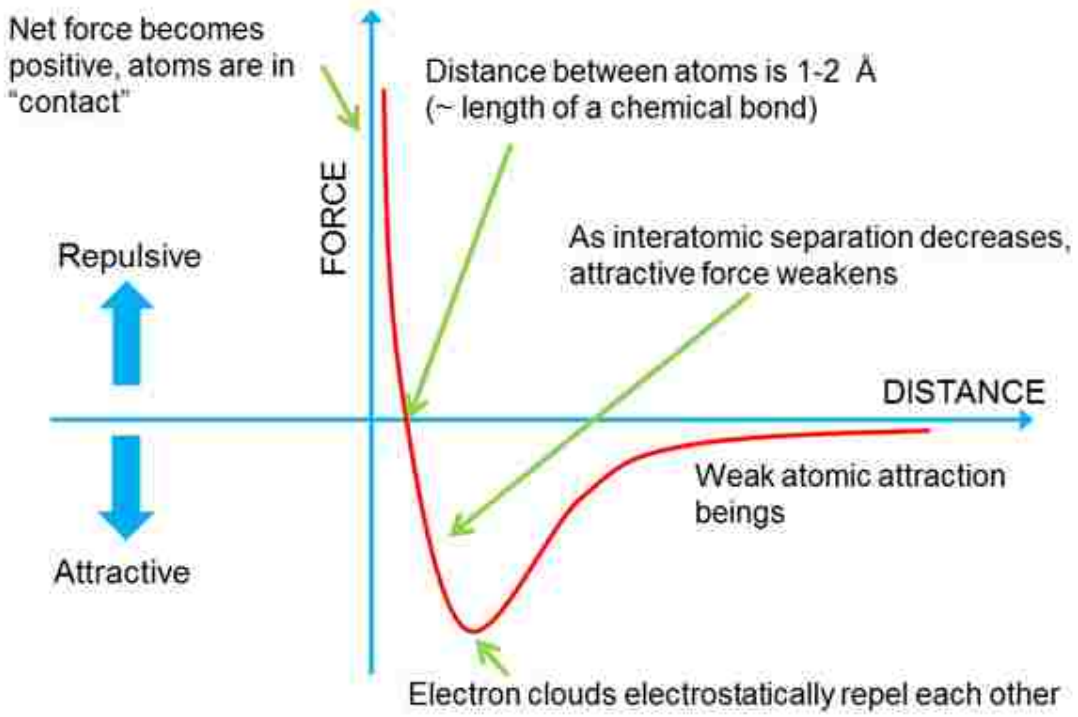

Figure 5: Force vs. distance curve[40]

2.3.2 Non-contact mode

Martin et al. developed non-contact AFM in 1987 [41]. In non-contact mode (NC-mode), the cantilever is oscillated above the sample surface in a resonant frequency with very low or constant amplitude of the order of few nanometers (<10 nm). This mode is also called oscillatory mode or dynamic mode. Here, the cantilever is oscillated at a resonant frequency. Depending upon the forces between the tip and sample, the cantilever resonant frequency changes. Tip-sample interaction in NC-mode is attractive as shown in the Figure 6. NC-mode can be classified into amplitude mode (AM) and frequency mode (FM) of operation. In the Amplitude mode (AM) of operation, the amplitude of the cantilever is kept constant, and the frequency remains close to its resonant frequency (which is fixed).

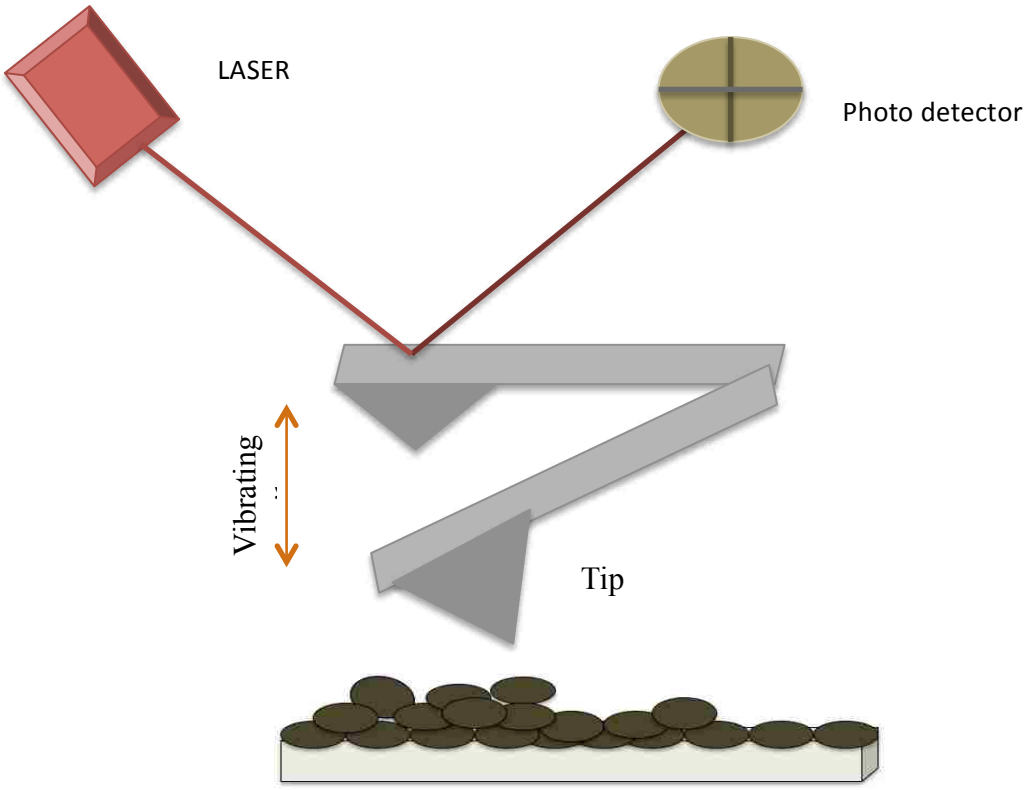

Figure 6: AFM in non-contact mode

When the tip is brought close to the sample surface, the tip sample interaction leads to changes in amplitude and phase of the cantilever. This mode is usually used to scan in liquid conditions. A high quality factor (Q) for the tip is necessary to obtain a high signal-to-noise ratio. High quality factor value can be achieved only in ultra-high vacuum (UHV) conditions, so this method is more suitable to a vacuum environment.

In the Frequency mode (FM) of operation, the cantilever is oscillated at resonance and continuously tracks the resonant frequency. The oscillation frequency of the cantilever changes with the change in resonant frequency due to tip-sample interaction. Using FM-AFM high atomic resolution images of sample surfaces can be obtained; it is generally oper-ated in UHV conditions.

In NC-AFM, as the tip approaches the sample the amplitude and phase of the cantilever changes, which results in a new frequency (f_{eff}) and new spring constant (K_{eff}) due to Van der Waals forces between tip and sample. The distance between tip and surface changes as Δd (not shown on figure) with changes in amplitude and phase as shown in the Figure 7. At the resonant frequency of the cantilever, the amplitude changes as ΔA, and the feedback loop compensates for Δd.

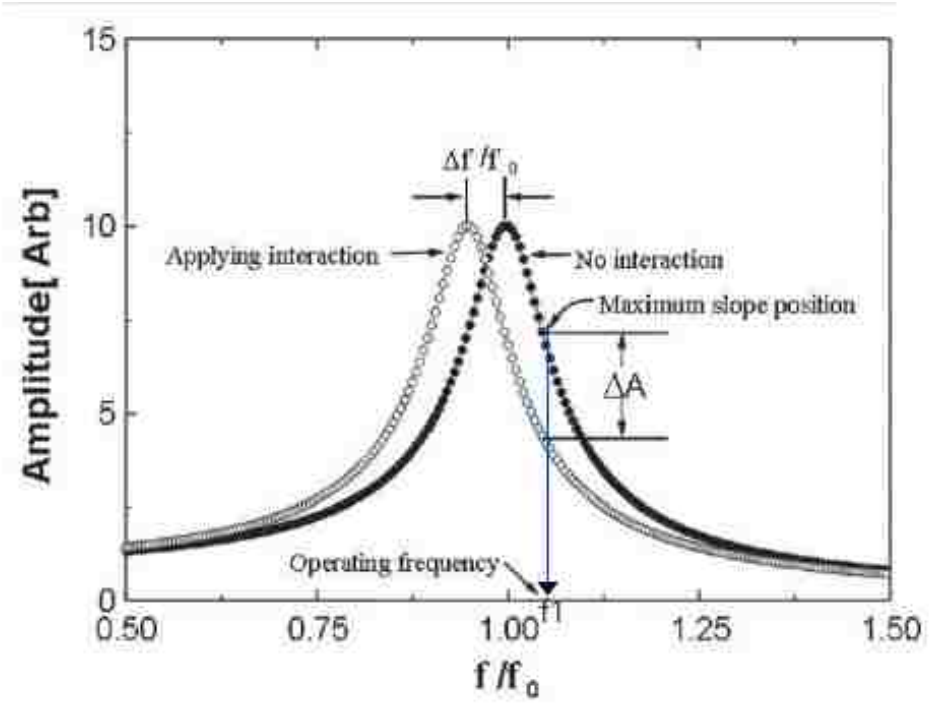

Figure 7: Resonant frequency shift when tip approaches the surface[42]

Some of the advantages of using non-contact AFM over contact AFM are as follows:

- Tip or sample surface does not experience any distortion as much less force is exerted on the sample surface.
- This mode can be used in both ambient and liquid environments.
- Visco elastic nature of the material can be studied.

Some of the disadvantages of using this mode are as follows:

- Higher resolution images cannot be obtained since the cantilever vibrates above sample surface.
- Higher signal-to-noise ratio.
- Contamination layer effects.

2.3.3. Tapping mode or Intermittent contact mode

This technique is similar to non-contact mode, where the cantilever is oscillated at a resonant frequency with higher amplitude with respect to the surface of the sample. Amplitude is usually kept constant in this mode. Therefore, this imaging technique is also known as amplitude modulation AFM (AM-AFM). Figure 8 illustrates the resonance curve of a cantilever above the surface and close to the surface of a sample (specimen). Tapping mode operates in the repulsive force region with periodic tapping on the sample surface. This technique is used to obtain high-resolution images of easily deformable material and loosely held substrates, which is difficult to image with regular AFM techniques. It also solves the problems with lateral forces and drag on the surface as the tip is touching only for short interval of time. Atomic resolution images of inorganic surfaces and high resolution images of polymers, isolated proteins, protein membranes can be obtained using this mode [43].

Tapping mode is performed with an amplitude modulation detector and a lock-in amplifier. Tapping mode can be performed in air, liquid, and vacuum. A strong cantilever and a considerably large oscillation amplitude is required while using tapping mode in air in order to overcome attractive capillary forces by the restoring force of the cantilever spring. The difference between amplitude and set-point determines the force between tip and sample and also determines the image. Tapping mode in liquid is used to scan biological samples.

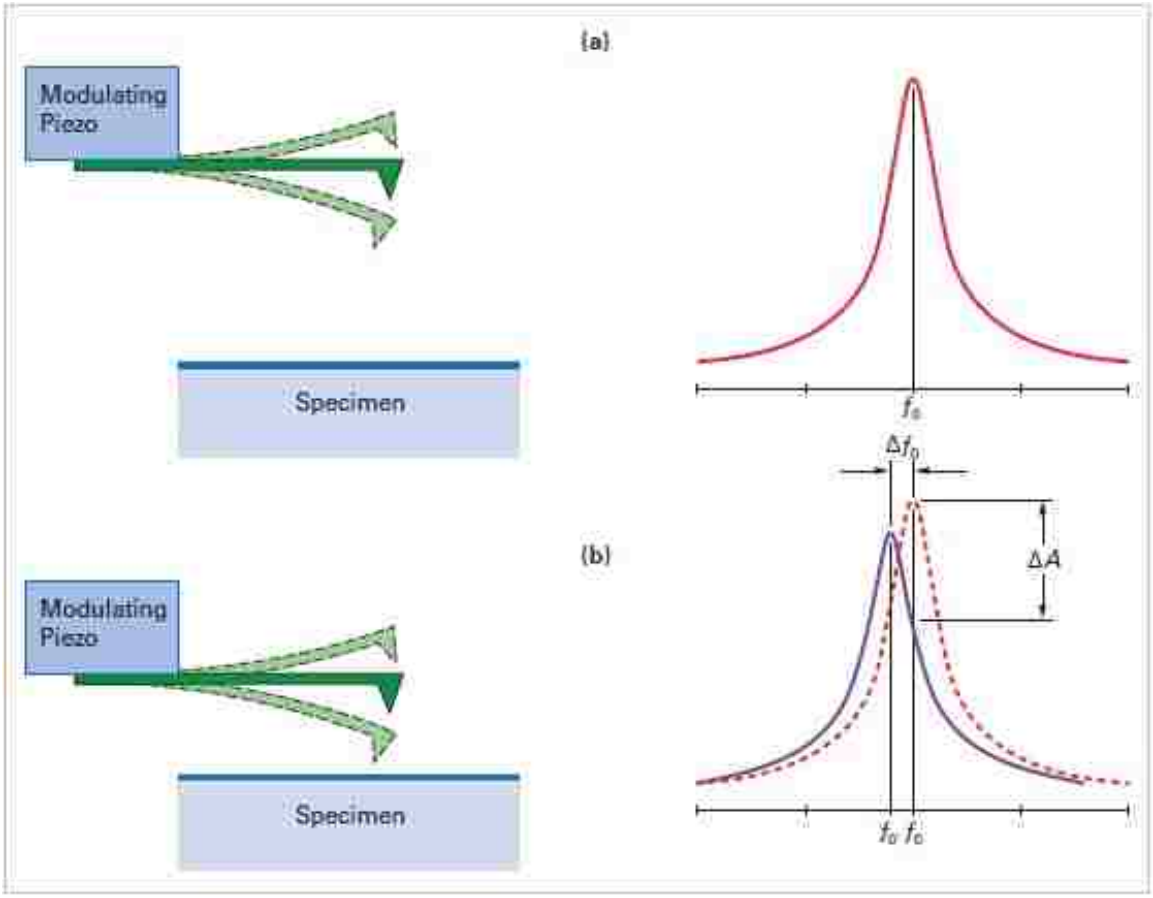

Figure 8: Resonance curve of cantilever (a) above the surface, (b) close to the surface[44]

By immersing the sample and the tip in liquid, adhesive capillary sample-tip problems can be reduced. The frequency of oscillation is kept constant near the resonance of the tip when force is applied on the cantilever by PZT (Piezoelectric tube). Piezoelectric tube comprises of X-Y piezoelectric ceramics and z-piezoelectric transducer (Figure 2). At this oscillation, the tip approaches the sample surface until the amplitude value is reduced to the set point value. Thus sample damages are minimized. The piezoelectric drive adjusts the Z-axis (vertical) position by keeping the oscillation amplitude at the set point. The changes in Z position of the tip are plotted as the XY position of the tip to obtain a height image.

Some of the advantages of using tapping mode AFM are as follows:

- This imaging technique can image samples that are loosely held to substrates.

- Minimizes problems associated with electrostatic forces, adhesion, and friction that are difficult to image in other scanning modes.

A primary disadvantage of this mode it that it is challenging to image single molecules using this technique.

2.4 Imaging Challenges and Limitations

Understanding the physical property of the material is one of the important criterions for the AFM imaging technique. Over the past few years AFM has been widely used in biological applications and to scan soft polymer materials given the normally minimal damage imposed by the instrument (particularly compared to other techniques) upon the sample under study. Used to scan single cells and the surfaces of living cells, this instrument can provide three-dimensional imaging and high resolution of real time images, all under various physiological conditions (related to the organism at the cellular or organ system level), with minimal sample preparation.

However, AFM has some limitations when used in the three different modes. In contact mode, the force exerted by the cantilever on the sample surface is high, which results in deformation of the sample surface. Applying smaller force and minimizing deflections can reduce sample damage [45], however, this must be balanced against effects upon image quality. The image contrast of a sample depends on the geometry of the probe. When the deflection of the cantilever is higher, the tip experiences more force. If the probe size is finite, it causes broadening of surface features which, in turn, leads to artifacts on images [45]. Imaging over sharp steps may also result in sample damage due to increase in forces between sample and repulsive tip [46].

One of the other limitations experienced by the user is sample preparation. While scanning biological samples, for example, the sample should adhere strongly to the substrate. While imaging living cells, the detachment of the cell is larger due to the reduced contact area between cell and substrate. To decrease this problem Dufrene has proposed an air-drying method which can be used to image yeast, bacteria, and fungal cells [45]. It is also difficult to obtain high resolution images of a cell surface in that it is a very soft sample. Another technique proposed by Dufrene is called the cell probe method[45]. In this technique cells are attached to the probe, and a force distance curve is recorded.

Interpreting the image is another challenging task in AFM studies. During ambient conditions the probe and the sample are sometimes contaminated which results in poor image quality. To determine the true profile of the surface, the shape of the probe tip must be controlled carefully, and its dimensions should be known accurately. Jacobsen and Helmersson suggest that tip effects must be taken into consideration while interpreting the data acquired [47]. The authors explicate an approach known as inverse AFM to acquire tip information with the obtained AFM images. If the objects seen in the images are steeper or sharper than the tip, then the approach is known as "inverse" AFM or "self" imaging which is similar to direct AFM imaging. This method provides information at each point as to where the tip is in contact with the sample during image acquisition [47,48]. To minimize the risk of inaccurate image analysis, Jacobsen and Helmersson also suggests in-situ examination of the tip regularly by means of inverse AFM using a sample surface which is known as a "tip characterizer" [47]. The ideal tip characterizer is an infinitely narrow spike, resulting in a perfect image of the tip.

With respect to certain specialized modes of operation, such as amplitude-modulation AFM (AM-AFM), imaging bistability (co-existence of both attractive and repulsive imaging

regimes) and mechanical sample damage are other operational challenges. Solares has proposed a new intermittent-contact AFM imaging concept known as frequency and amplitude modulation atomic force microscopy (FAM-AFM) [49]. This imaging method is a combination of existing non-contact frequency-modulation atomic force microscopy (FM-AFM) and AM-AFM. FAM-AFM uses a new control scheme based upon a variable excitation force amplitude and frequency to control the cantilever effective frequency and limit the magnitude of tip-sample forces. Limiting the magnitude of tip-sample interaction forces helps to decrease the potential mechanical damage of samples. Also, the cantilever is continuously excited at variable frequency so that bistability is eliminated [49].

Thus, an enormous amount of research has been carried out to overcome the challenges and limitations of AFM. Discussed above are some of the commonly used techniques to enhance image resolution, to interpret images in effective way, to decrease bistability, and to protect samples from damage.

2.5 Conductive Probe AFM (CP-AFM)

CP-AFM is one of the tools used to obtain electrical and structural characteristics of nanostructures. Simultaneous electrical properties and topographical information of the sample can be obtained from this instrument, which makes this a very efficient and versatile tool. To image the sample surface a conductive tip is used which acts as one of the electrodes, and a conductive substrate or any other conductive material on the substrate acts as a counter electrode. Very low voltage is applied in between these two electrodes, and a corresponding current up to the micro Amp (μA) range can be measured. With this technique it is possible to obtain current-voltage characteristics (I-V), current-vertical distance characteristics (I-Z),

and also the local conductivity of a sample. A schematic diagram of a CP-AFM setup is shown in Figure 9.

Figure 9: Schematic a of conductive probe AFM system

To obtain the I-V characteristics of a nano object, the tip is held fixed at a point, and tip-sample voltage is increased. For I-Z measurements, the bias across the sample is kept constant, and a scanner is moved along z-direction. In this thesis, we characterize HEMs using CP-AFM

2.6 Raman Spectroscopy

Raman spectroscopy is a technique based on the inelastic scattering of monochromatic light as is typically provided by a laser source in the near infrared, visible, or ultraviolet range. Inelastic scattering, by definition, involves a change in energy or, in this case, a shift in the frequency of incident photons as they interact with the sample. Specifically, as light from the aforementioned monochromatic source impinges upon a sample, the photons interact with the quantized molecular vibrations (i.e.-phonons in crystalline solids) of the material. As a result, the photons are absorbed by the sample and reemitted in an inelastic scattering event. By comparison to the original monochromatic frequency, the frequency of the reemitted photons is shifted up or down. This change in frequency is called the Raman effect.

This Raman shift provides vibrational, rotational, and other low frequency information about the sample[50]. Raman effects are based on molecular deformation in an electric field 'E' which is determined by molecular polarizability 'α'. The laser beam can be considered as an oscillating electromagnetic wave with electric vector 'E'. Upon interaction with the sample it induces an electric dipole moment P= αE which deforms molecules. Due to periodical deformation molecules vibrate with frequency 'ν_m'. Monochromatic laser light with frequency 'ν_o' excites molecules and transforms them into oscillating dipoles. The oscillating dipoles emit light of three different frequencies [51].

Rayleigh Scattering: In this interaction, molecules with no active mode absorb a photon with the frequency 'ν_o'. The excited molecule returns back to the same basic vibrational state and emits again with the frequency 'ν_o' as an excitation source.

Stokes scattering: Raman active molecules absorb a photon with the frequency 'ν_o' Part of the photon energy is transferred to the Raman active mode with the frequency 'ν_m', and the resulting frequency of scattering light is reduced to '$\nu_o - \nu_m$'.

Anti-Stokes scattering: Raman scattering molecules absorb a photon with the frequency 'ν_o'. At the time of interaction photons are already in the excited vibrational state. Excessive energy is released by the excited Raman active mode, and molecules return to basic vibrational states. The resulting frequency of scattered light goes to '$\nu_o+\nu_m$'. Only about 0.001% of the incident light produces the inelastic Raman signal with frequency '$\nu_o \pm \nu_m$', and about 99.999% of all incident photons in the spontaneous Raman process undergo elastic Rayleigh scattering. Spontaneous Raman scattering is very weak and measures should be taken to distinguish it from Rayleigh scattering. Instruments such as notch filters, tunable filters, double

and triple spectrometric systems, and laser stop apertures are used to reduce Rayleigh scattering and to obtain high quality Raman spectra[51].

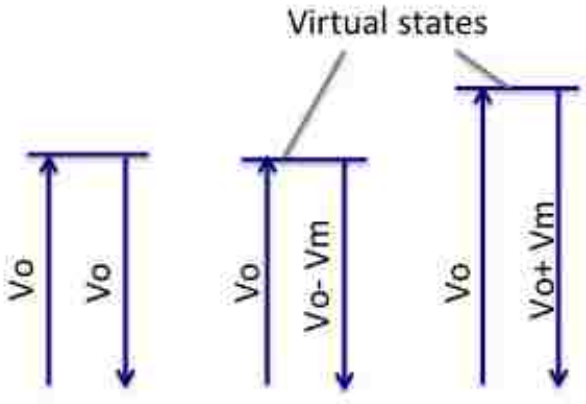

Figure 10: Raman transitional mode

The equipment used to perform Raman spectroscopy consists of an excitation source (laser), a sample illumination system and light collection optics, wavelength selector (filter or spectrometer), and a detector (photodiode array, CCD, or PMT). For this thesis, Raman spectroscopy was used to find vibrational states of two different hybrid materials. The peaks at different positions corresponding to wavenumbers are analyzed and results are discussed. This technique is an important means by which to better understand the complex characteristics of HEMs.

2.7 Scanning Electron Microscopy

A Scanning Electron Microscope uses a focused beam of electrons to generate signals on the sample surface. The signals obtained from electron-sample interactions disclose in-

formation about sample external morphology, orientation of the material, chemical composition, and the crystalline structure of the sample.

In SEM, a beam of electrons is produced by an electron gun. This electron beam follows a vertical path through the microscope, electromagnetic fields, and lenses, and is then focused onto sample. These accelerated electrons have high kinetic energy when they interact with the sample. In turn, secondary electrons, backscattered electrons, diffracted backscattered electrons, and x-rays are ejected. A detector collects the secondary and backscattered electrons that produce the final image. Using SEM, we can obtain the morphology and topology of the sample surface, in general, while backscattered electrons provide composition information in multiphase samples, in particular.

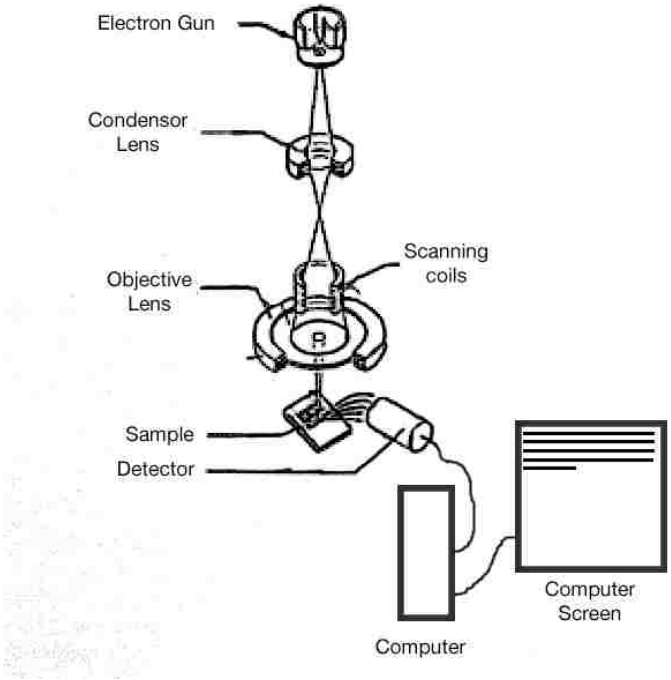

Figure 11: Schematic diagram of Scanning Electron Microscope (SEM)[52]

2.8 Limitations of SEM

- Only solid samples of certain dimension fit inside the chamber.
- An electrically conductive coating must be applied on insulating samples to study them.
- Operates in vacuum; very expensive instrument.

3. CHARACTERIZATION OF RHODAMINE 6G TETRAPHENYLBORATE ([R6G][TPB]) GUMBOS

3.1 Introduction to GUMBOS

A Group of Uniform Materials Based on Organic Salts (GUMBOS) are ionic liquids that are defined as organic salts with melting points above 100^0 C [17]. Prior to the discovery and synthesis of these unique materials, the interest in ionic liquids was due to their ability to act as solvents for a wide variety of materials such as organic, inorganic, and organometallic compounds. Traditional ionic liquids are composed of a wide range of sizes of anions and bulky organic cations. They have unique physical and thermodynamic properties, such as negligible vapor pressure, low flammability, and high electrochemical and thermal stability. Frozen ionic liquids, which are of our interest, are defined as ionic liquids with melting points above room temperature. Professor Isiah M. Warner (LSU, Department of Chemistry) reported the first micro and nanoscale particles derived from frozen ionic liquids [16]. Later given the moniker of GUMBOS, these materials have all of the prominent properties of ionic liquids but now, through functionalization of cations and anions, can be synthesized to exhibit fluorescence [17, 20, 22], magnetic susceptibility [18], and antimicrobial effects [23, 53]. Thus, GUMBOS have been described as "designer nanoparticles." Their tunability, via the chemical manipulation of anion-cation pairs to exhibit the aforementioned properties, make GUMBOS a likely candidate for future HEM device development.

3.2 Synthesis of GUMBOS

GUMBOS can be synthesized in the form of nanorods/nanoparticles/ nanowires which exhibit properties such as fluorescence, magnetic susceptibility, and antimicrobial ac-

tivity [54]. Even though, the focus of our work is primarily upon the characterization of rhodamine 6G tetraphenylborate ([R6G][TPB]) GUMBOS, it is necessary to know background information and a brief description of the primary steps for synthesizing these materials as given below.

3.2.1 Melt-emulsion-quench technique with and without emulsifying agent

Tesfai et al. first reported this technique in 2008. An oil-in-water (o/w) microemulsion approach was used in the preparation of uniform and frozen (ambient-stable solid) ionic liquids micro and nanoparticles [16]. The ionic liquid of 1-butyl-2,3 dimethylimidazolium hexafluorophosphate ([bm_2Im][PF_6]), with a melting point of 42°C, was used as the starting material for each of two methods. The first method involves the melting and subsequent o/w dispersion of liquid phase ([bm_2Im][PF_6]) into water above the melting point of the ionic liquid. This step is followed by fast cooling to form discrete solid ionic liquids as shown in Figure 12. In the second method non-ionic surfactant Brij 35 is used instead of [bm_2Im][PF_6].

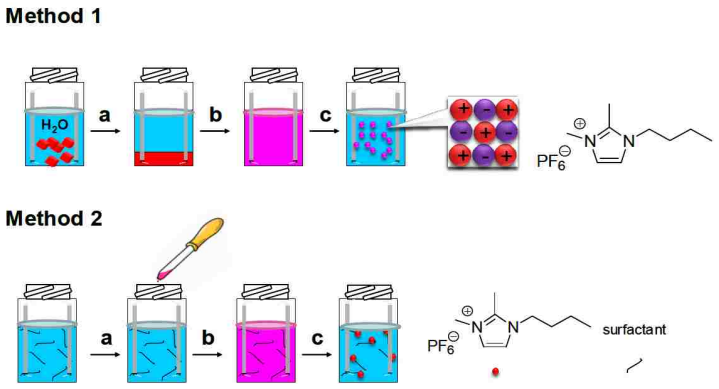

Figure 12: Steps for melt-quench-emulsion technique. Synthesizing nanoparticles using no surfactant and without emulsifying agent (Method1) and using surfactant and emulsifying agent (Method2). (Reprinted with permission from reference 16 and corresponding author I.M. Warner. Copyright (2008) American Chemical Society. See Appendix B)

3.2.2 Reverse micelle synthesis

This technique uses two precursor salts for the ion exchange reaction. Two identical water-in-oil emulsions are mixed together using the precursor salts. These two emulsions are combined in a 1:1 ratio, and particles are formed by diffusion followed by an ion exchange reaction [18]. Particle sizes can be controlled by varying the concentration of the solution. The following figure illustrates the steps for the reverse micelle technique.

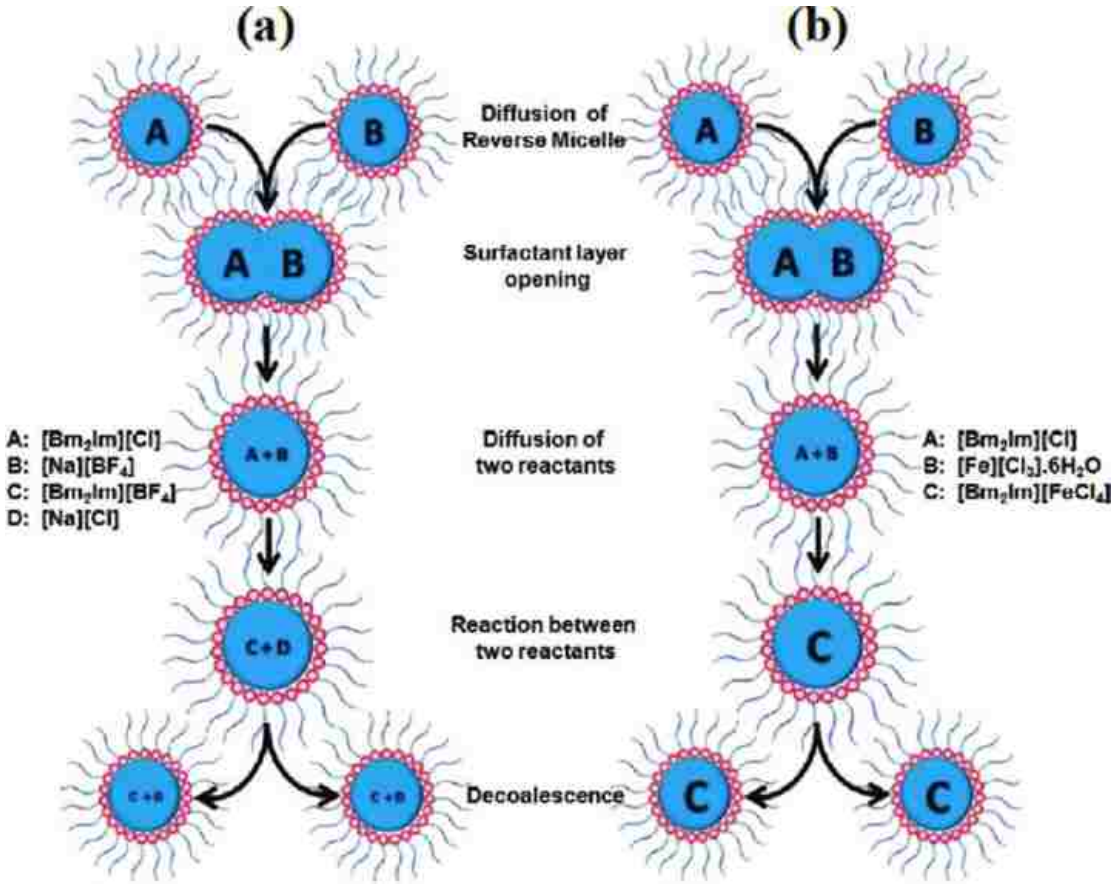

Figure 13: Represents reverse micellar templating method for synthesis of (a) [Bm2Im][BF4] nanoGUMBOS (b) [Bm2Im][FeCl4] magnetic GUMBO paricles. (Reprinted with permission from reference 18 and corresponding author I.M. Warner. Copyright (2008) American Chemical Society. See Appendix B)

3.3 Rhodamine 6G Tetraphenylborate([R6G][TPB])

The chemical structure of ([R6G][TPB]) is shown in the Figure 14**.** Rhodamine 6G Tetraphenylborate ([R6G][TPB]) is prepared by anion exchange reaction starting with the precursor salts, Rhodamine 6G chloride ([R6G][Cl]) and sodium tetraphenylborate ([Na][TPB]). [R6G][TPB] GUMBOS are obtained by metathesis reaction in a biphasic mixture of water and dichloromethane (DCM). GUMBOS thus obtained are rinsed several times with DI water, which removes NaCl by-products. Dried [R6G][TPB] GUMBOS are obtained after drying out all the dichloromethane solvents.

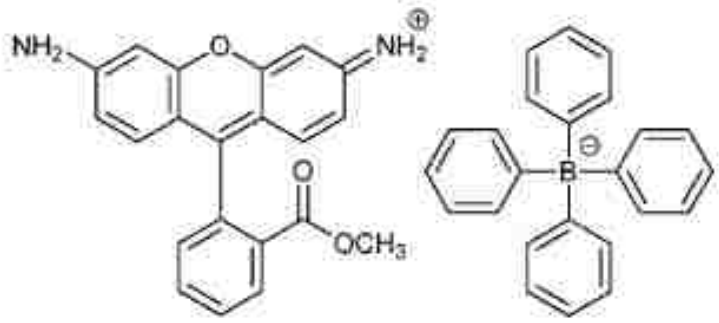

Figure 14: Chemical structure of [R6G][TPB] (Reprinted with permission from reference 33 and corresponding author I.M. Warner. Copyright (2011) Royal Society of Chemistry. See Appendix B)

[R6G][TPB] nano particles are prepared using the melt-quench- emulsion method as discussed in section 3.2.1. A 100µL of 1mM [R6G][TPB] ethanol solution is added to 5mL of DI water, and the resulting solution is sonicated for 5 minutes. Water and ethanol are filtered prior to the preparation of nanoparticles using 0.45µm nylon membrane filter. The nanoparticles thus obtained are suspended in DI water for 1hour in the dark.

3.3.1 Sample preparation for AFM imaging

Sarkar et al. describes the sample preparation for [R6G][TPB] nanoparticles in their article, "Electro-optical characterization of nanGUMBOS" [54]. [R6G][TPB] nanoparticles were deposited on two different substrates (gold coated on glass or a silicon substrate). A drop casting technique was used to deposit the nanoparticles onto these different substrates. To minimize agglomeration of particles in the solution, the solution containing the [R6G][TPB] nanoparticles was placed in an ultrasonic bath for 15 minutes prior to deposition onto the substrates. The droplets that were dispensed on the substrate were allowed to dry in ambient air for 24 hours before performing any experiments on them [55].

3.3.2 Atomic force microscopy (AFM) imaging of [R6G][TPB] nanoparticles

AFM imaging was conducted in contact mode using a Micromasch manufactured CSC17/AlBS probe. The probe used was composed of n-type silicon with an aluminum detector coating and cone angle of 40^0. A force constant of 0.18N/m was applied to the sample. The force applied by the probe varied from 0.06 to 0.14 N/m depending upon the type of substrate upon which the sample was deposited. Tips with low stiffness are used to interact directly with the surface of the sample in the contact mode, as they are more flexible and can adapt to the varying terrain, and are sensitive to minute forces when compared to the stiffer tips used for vibrating modes. Different areas on the sample were imaged using raster scanning with different magnifications. Due to the drop casting technique, a considerable amount of agglomeration can be observed. Although the solution was placed in an ultrasonic bath (as described in 3.3.1) to minimize agglomeration, a considerable amount of the latter remains for these samples in this section. Figure 15 shows the AFM images of [R6G][TPB] nanoparticles. In order to find the thickness and the height of the nanoparticles, we have employed

Line Scan Analysis (LSA) tool available in the AFM software. When AFM is used to scan topography, it uses the tip to scan the area line by line, causing the tip to track the three dimensional changes of the surface. Line scan extracts the data from the three dimensional information obtained by the tip for analysis. Using the analysis software of Pacific Nanotechnology, the manufacturer of our AFM, it was found that the diameters of these particles varied from 200 to 500 nm.† The variation in height observed is due to the stacking of the nanoparticles. Size variation in the formation of the particles is due to the inherent nature of the method used in their synthesis.

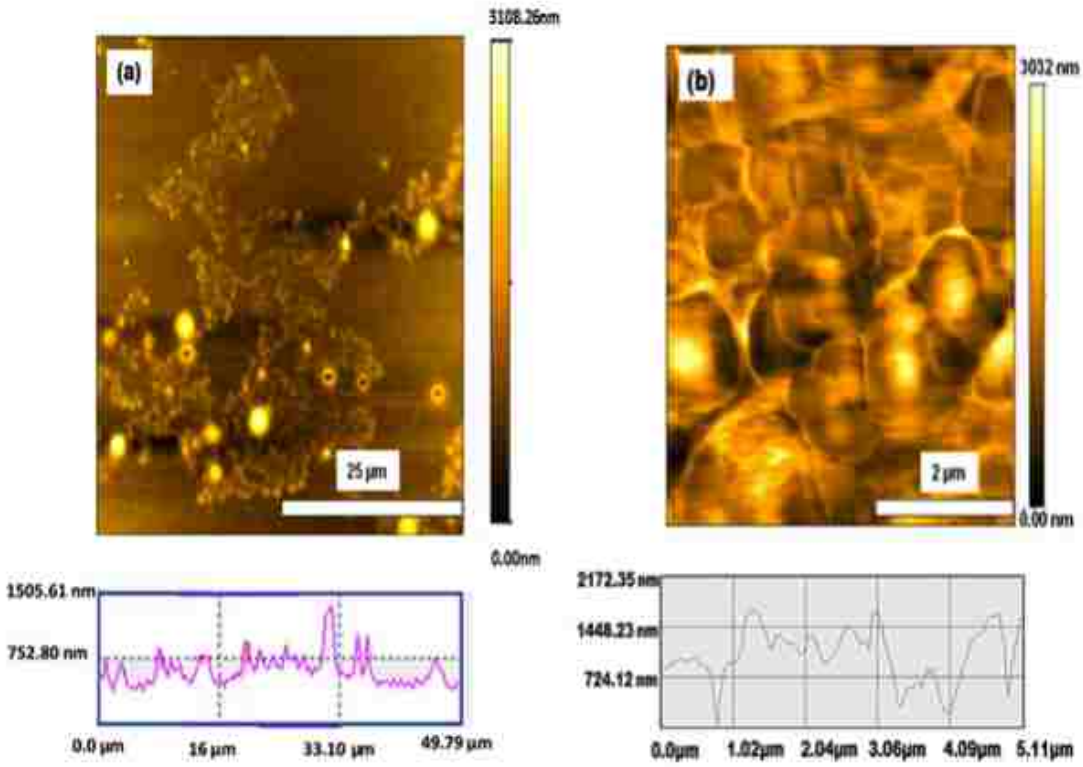

Figure 15: AFM images of [R6G][TPB] nanoGUMBOS (a) topography image of dropcasted [R6G][TPB] nanoparticles on gold surface (scan area: 50 µm x 50 µm) (b) image of nanoparticles (scan area: 5 µm x 5 µm) [54].

† Although the term "nano" is typically reserved for structures of < 100nm in a given dimension in both the EE and Physics literature, some latitude must be allowed with respect to the definition of nanoscale dimensions, as per the Chemistry literature upon which these samples are based.

When a 10.21 x 10.21 μm^2 area is scanned, the [R6G][TPB] molecules are distinctly visible without any significant agglomeration. Figure 16 shows the AFM image of 10.21 x 10.21 μm^2 area. Our analysis showed that the roughness of this area was in the 130.97nm range.

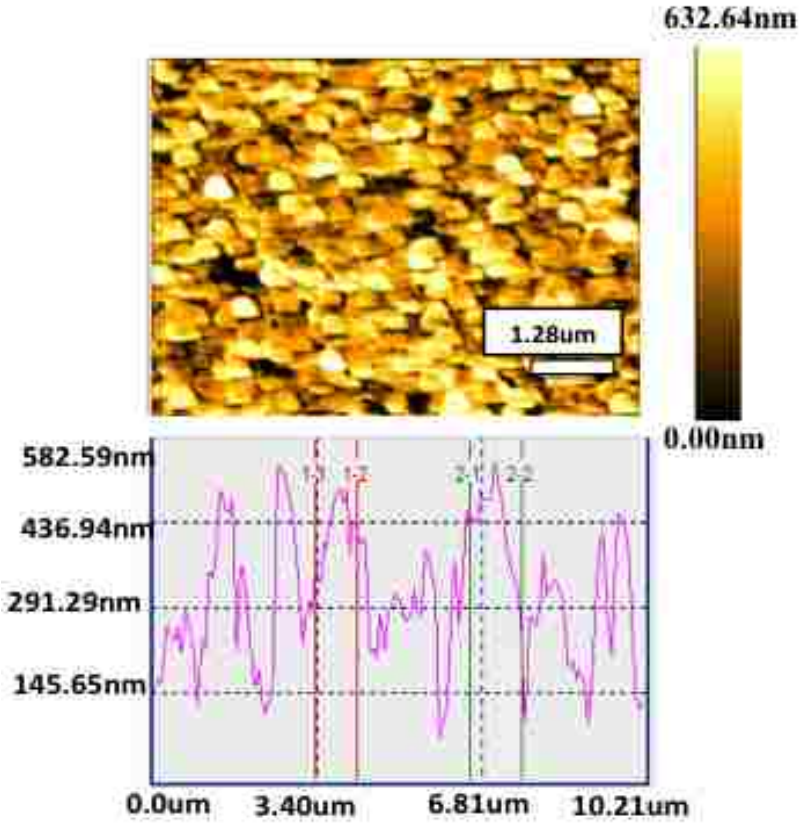

Figure 16: AFM image obtained when scanned on a 10 μm^2 area.

3.4 Contact Probe (CP-AFM) Measurement of [R6G][TPB] GUMBOS

A Keithley 4200 Semiconductor Characterization System (SCS) was used to find current-voltage (I-V) characteristics. Here, an AFM tip coated with platinum was used as one electrode and a gold substrate was used as the other electrode. A limiting current is passed through the tip as high currents have a tendency to damage the tip. External resistors are also used to limit the current flowing through the tip.

The tip is lowered until it touches the nanoparticles. A constant voltage of approximately of 0.25 V is applied, and the tip is moved towards the [R6G][TPB] nanoparticles surface in small increments to find out if any changes in current are observed. When current values change, the voltage is swept from 0 to 1V in 0.05V increments using the SCS. A corresponding current is measured for the different voltage values. Thus, tip is moved in different positions throughout the sample surface, and I-V measurements are made. The current values ranged from approximately 10^{-6} to 10^{-7} A, and resistance was calculated to vary from 0.3M to 3MΩ. Figure 17 shows I-V characteristics of [R6G][TPB] nanoparticles.

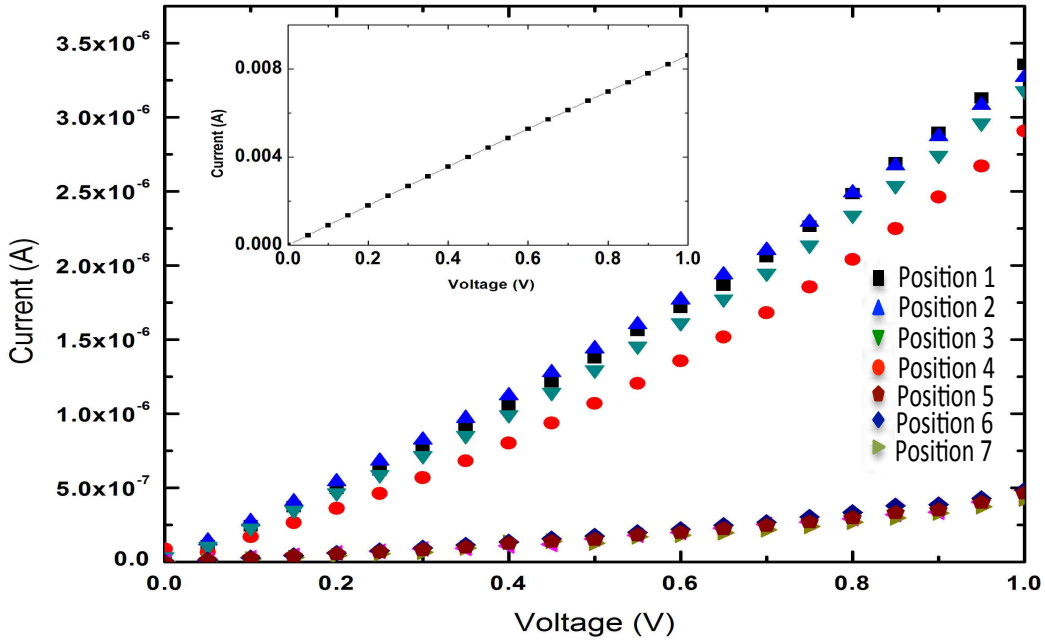

Figure 17: I-V characteristics of [R6G][TPB] nanoparticles with CP-AFM. Inset figure shows I-V characteristics of the platinum coated tip directly in contact with gold surface that was used for reference.

The blue, red, and brown traces in the figure represent I-V characteristics of nanoparticles measured at various locations on the substrate. The non-linearity in the I-V relationship obtained in the figure is due to sensitivity in various factors such as the aggregation of parti-

cles, interaction at the substrate-nanoparticle interface, and the injection of charges (or current flow due to electron tunneling) through the nanoparticle-tip-junction barrier [54]

3.5 Conclusions

Atomic Force Microscopy and conductive probe AFM experiments were successfully performed on new class of materials, known as GUMBOS. With AFM images, the diameter of each particle was found to be in the 200-500nm range, and current values obtained from CP-AFM measurements were approximately 10^{-6} to 10^{-7} A, when scanned from 0 to 1V. The junction resistance value was found be in the 0.3 to 3MΩ range. The main advantage of using GUMBOS in electronic applications is the ease of synthesis of nanoparticles from parent compounds, and also, by varying the anionic or cationic component in their structure, high thermal and adaptable functionality can be achieved [54]. However, work remains in terms of integrating the versatility of these materials to a deposition (or subsequent fabrication) method(s) and particle sizes that will be amenable to device processing and development beyond the characterization phase.

4. CHARACTERIZATION OF 3-AMINOPROPYLTRIETHOXY SILANE (APTES) DEPOSITED ON SILICON SUBSTRATES

4.1 Introduction to APTES

Aminopropyltriethoxy Silane (APTES) is used as an effective silane (SiH_4) coupling agent on several substrates to enhance adhesion. Lyubchenko and co-workers used APTES to functionalize mica surfaces with amine groups which protonates at neutral PH [56]. Later, Karrasch et al. introduced an additional cross linking group at the amino end of APTES on glass substrates [57]. Due to its ability to form strong covalent bonds with proteins and inorganic surfaces, the morphology, thickness, and conformation of APTES are of great interest [58]. The chemical structure of APTES is shown in the Figure 18

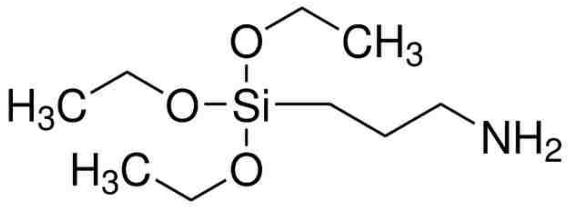

Figure 18: Structure of APTES

There are numerous methods to deposit APTES on different surfaces. The conventional method of film formation of APTES on silicon substrates is by the formation of silanols. Hydrolysis of ethoxy groups in APTES catalyzed by water forms silanols. A monolayer of APTES is formed when APTES silanols are condensed with surface silanols, and in this case amino group are oriented away from the silicon substrates. Anhydrous toluene and phosphate-buffered saline can also be used to prepare an APTES solution [47]. APTES is also used as a coupling agent in glass fibers, coatings, adhesive joints, and for covalently binding proteins to inorganic surfaces [48a].

In this thesis, we have investigated the morphology of APTES deposited on silicon substrates using AFM. Note that a separate study was conducted in our group with respect to carbon nanotube (CNT) deposition, using electrophoretic deposition (EPD), upon APTES functionalized silicon substrates [59]. However, those details are outside of the scope of this thesis. For this project, the effect of varied APTES concentration (5-50%) was studied, and results were noted before the deposition of CNTs.

4.2 Sample Preparation

Different concentrations of APTES were prepared by the appropriate dilution of 95% of ethanol and DI water [59]. For example, in order to prepare a 20% APTES solution, 2 ml of APTES were mixed with 2 ml of DI water and 6 ml of ethanol.

The deposition of APTES is a challenging task as it often results in multilayer deposition and has the tendency to form uneven surfaces. There is a possibility that this material undergoes certain chemical changes and also can be stripped from the surface due to presence of the aqueous solution, indicating that there is a lack of covalent bonding [58]. The type of solvent, concentration, reaction temperature, and reaction time are some of the parameters that should be considered prior to deposition [60]. Care should be taken to obtain a smooth deposition, thus avoiding agglomeration and incomplete coverage.

In this work, the surface functionalization of silicon substrates is achieved by a process of self-assembly by the APTES monolayer. Silicon wafers of $1cm^2$ were cut and cleaned in the presence of oxygen for 30 minutes, followed by immersion in piranha solution (2:1 sulfuric acid to hydrogen peroxide) for 30 minutes. This establishes a substantial number of hydroxyl (-OH) groups by the process of hydroxylation. A salinization step involves hydrolysis of ethoxy ($-C_2H_5$) groups from APTES molecules, which forms silanols (Si-O-H). The

APTES silanols condense with surface silanols resulting in the self-assembling of a monolayer of APTES by lateral siloxane (Si-O-Si) arrangement. In the self-assembled siloxine arrangement, it can be observed from the figure that the positively charged amine groups ($-NH_2^+$) are positioned away from the silicon substrates.

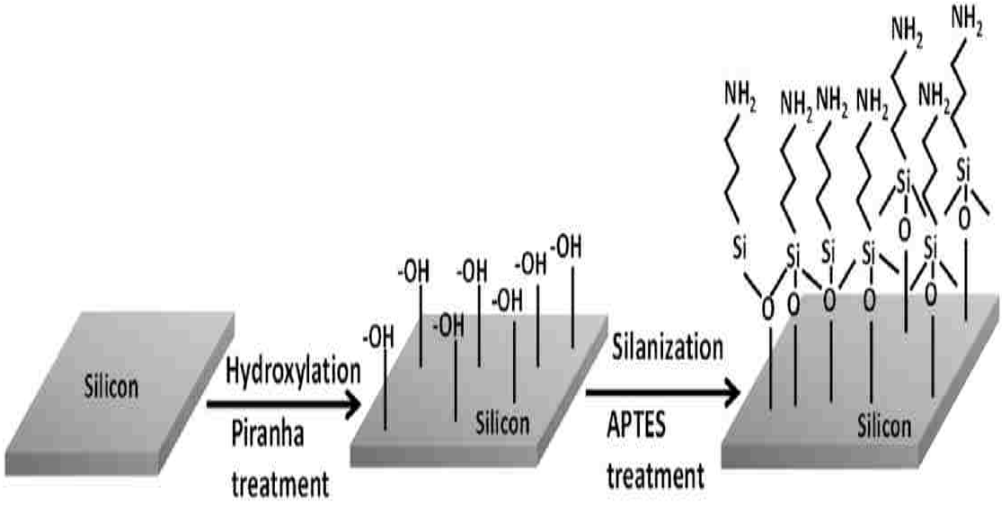

Figure 19: Schematic diagram showing the hydroxylation after piranha treatment and salinization by 3-aminoprooyl-triethoxysilane (APTES) treatment on silicon substrate [59].

Using the above mentioned technique different concentrations of APTES varying from 5% to 50%, were prepared.

4.3 Characterization of APTES Molecules of Varying Concentrations on Silicon Substrates Using Atomic Force Microscopy

Atomic Force Microscopy images were obtained in contact mode. AFM experiments were performed using a 450 μm long and 50 μm wide silicon cantilever with aluminum detector coating, a stiffness 0.18N/m, and a cone angle 40^0. The force applied by the probe varied from 0.06 to 0.14 N/m depending on the type of material deposited on the substrate.

4.3.1 Roughness analysis of APTES on bare Si substrates

Roughness analysis is a relative height analysis. The arithmetic roughness average, 'R_a' values, and the root mean square roughness, 'R_q', were applied to calculate the roughness analysis. The equations, $R_a = \frac{1}{n}\sum_{i=1}^{n}[\text{hi} - (\text{h})]$ and $R_q = \sqrt{1/n}\sum_{i=1}^{n}[h_i - (\text{h})]$ were used, where n is the number of data points, Ra is the average distance between the i^{th} height (h_i) to the mean height (h) of all n data points. Rq is the standard deviation, i.e. the root mean square distance between the i^{th} height (h_i) to the mean height (h) of all n data points.

A scan size as high as 50 μm was used initially in order to visualize the large area. Eventually the scan size was decreased from 30 μm to 15 μm, 5 μm, and finally to 1 μm to be able to resolve all features. When scanned with the 50% APTES concentration on silicon (substrate), the average roughness and diameter of the particles were approximately found to be 360 nm and 0.5 μm, respectively. Figure 20 illustrates the AFM images and corresponding line profiles of 4.5 x 4.5 μm^2 and 2.5 x 2.5 μm^2 scanned areas, respectively. In another set of experiments, a 20% APTES concentration was deposited on silicon substrates and was imaged using AFM. When scanned with 50% APTES concentration on silicon substrate, the average roughness and diameter of the particles were approximately found to be 230 nm and 0.5 μm, respectively. The images showed that the average diameter of the molecules are 0.5 μm, Figure 21 shows these AFM images and their corresponding line profiles. When the standard deviation was computed for these various concentrations of APTES on silicon strates, it was found out to be 12% of the mean and 15% of the mean for 50% and 20% concentrations, respectively indicating uniform distribution of APTES solution on the substrates.

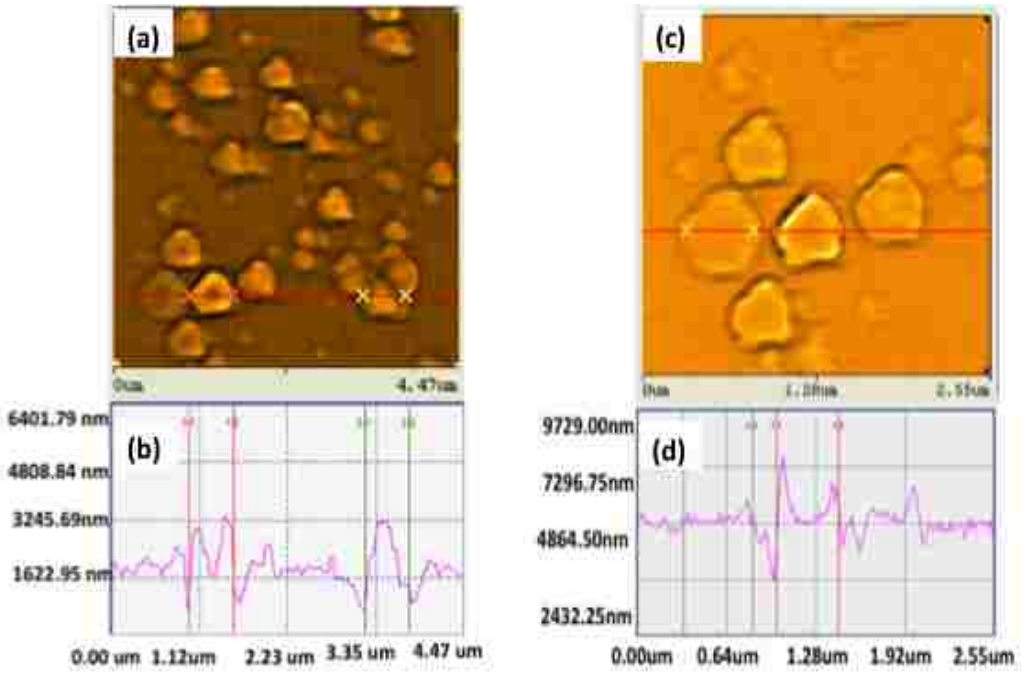

Figure 20: Morphology of 50% APTES film (a) 4.5 μm^2 scanned area (c) 2.5 μm^2 area, which is small scale of (a). Panels (b) and (d) represent line profiles of (a) and (b), respectively.

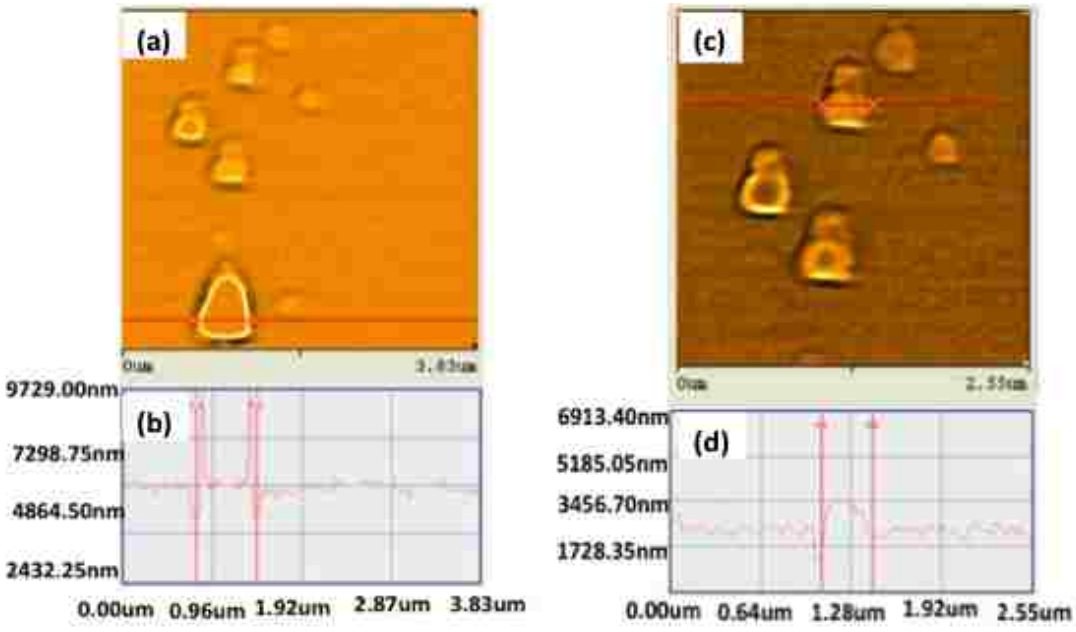

Figure 21: AFM image of 20% APTES concentration (a) 3.8 μm^2 area, (c) 2.5 μm^2 area, which is smaller area of (a). Panels (b) and (d) show line profiles of (a) and (b), respectively.

4.3.2 Roughness analysis of APTES on Si intended for carbon nanotube (CNT) deposition

Varying concentrations of APTES were deposited on silicon substrates with the intention of depositing CNTs to examine the binding capability of CNTs with different APTES concentrations. The thickness of the CNTs deposited on the silicon surfaces may vary depending upon the APTES concentration. Experiments indicate a non-linear variation between the CNT thickness and APTES concentration. A significant increase in the thickness of CNT deposition was observed for APTES concentrations in the range of 0% to 20 %. However, beyond an APTES concentration of 20%, only marginal variations in the CNT thickness were observed. For example, for an applied electric field of 10 V/cm, and a deposition time of 3 minutes, an increase in APTES concentration from 5% to 20% resulted in the increase of CNT deposition thickness from 0.8 μm to 2.0 μm. However, for the same applied electric field and time, a further increase in APTES concentration from 20% to 50%, resulted in only marginal increase in the CNT deposition thickness from 2.0 μm to 2.3 μm. For the APTES concentrations in the range of 50%-100%, negligible differences in the CNT deposition thickness were observed due to saturation[59]. The saturation of CNT deposition thickness at high APTES concentrations (50%-100%) stems from a drastic reduction in inter-electrode electric fields due an increased presence of organosilane compounds on the silicon substrate. Thicknesses were measured using KLA-Tencor alpha step surface profiler.

4.4 Raman Spectroscopy Analysis of APTES Molecules

APTES molecules deposited on silicon substrates were examined using Raman spectroscopy. For measurements, a HeNe laser with a wavelength of 638.4 nm and an incident power of 17mW was used. The confocal hole aperture of 200 μm and a grating of 1800 lines per

mm were selected in the Jobin Yvon Horiba Labram Raman spectrometer used in this study. Scans were performed in the range of 100 to 3000 cm^{-1} using a 100x objective. Beams were focused on the surface of the APTES film with different concentrations, and the results were examined.

Recall that as discussed in section 2.5, Raman spectroscopy is a technique based upon the inelastic scattering of monochromatic light. With Raman spectroscopy, vibrational, rotational, and other low frequency information can be obtained. For these samples the inelastic scattering of the incident HeNe laser light leads to a change in frequency of photons that have interacted with the given sample. In the subsequent interaction and comparison between the absorbed and reemitted photons, a change in frequency, known as the Raman effect is measured.

For our samples, we examined the Raman spectra of APTES concentrations of 50% and 20% as shown in Figure 22. Once again, these APTES molecules were also under investigation in a separate (but related) study on EPD in our group on the electrophoretic deposition (EPD) of CNTs using APTES functionalized substrates[61]. However, the Raman spectra obtained for this thesis provide sample composition data, beyond the AFM results, as are needed for our overall study of the morphology of this material. An inset of the Raman spectrum for bare Si (also shown in the figure) clearly indicates the successful deposition of APTES upon these samples. For both the 50% and 20% APTES concentration samples, we observed strong peaks at 940 cm^{-1}. These are due to C-C stretching vibrations. Moreover, in this case a Raman peak at 940 cm^{-1} is due to the presence of α-helical confirmation (stretching of amino acid)[62]. The strong peak at 520 cm^{-1} corresponds to Si-O-Si network vibrations. Likewise, the strong peak at 520 cm^{-1} is due to the creation of "triply degenerate", long wave-

length “transverse optical phonons” [63]. N-H bond stretching is expected at 3310-3370 cm^{-1} [64]. The vibrations involving N-H stretching are due to strong IR absorption [65]. However, due to limitations of the spectrum range used, these latter bands above 1900 cm^{-1} could not be captured. With the exception of portions of the traces below approximately 100 cm^{-1} and above 1000 cm^{-1}, the intensity of the 20% APTES solution is slightly higher than that of the 50% solution. This may be due to the higher absorption coefficient of the materials containing 20% APTES. The absorption coefficient depends on the type of material and wavelength of light that is being absorbed. Since, a 20% APTES solution has a slightly lower coverage across a silicon surface compared to a 50% APTES solution, the intensity of the 20% APTES solution peak is slightly higher than 50% APTES solution peak.

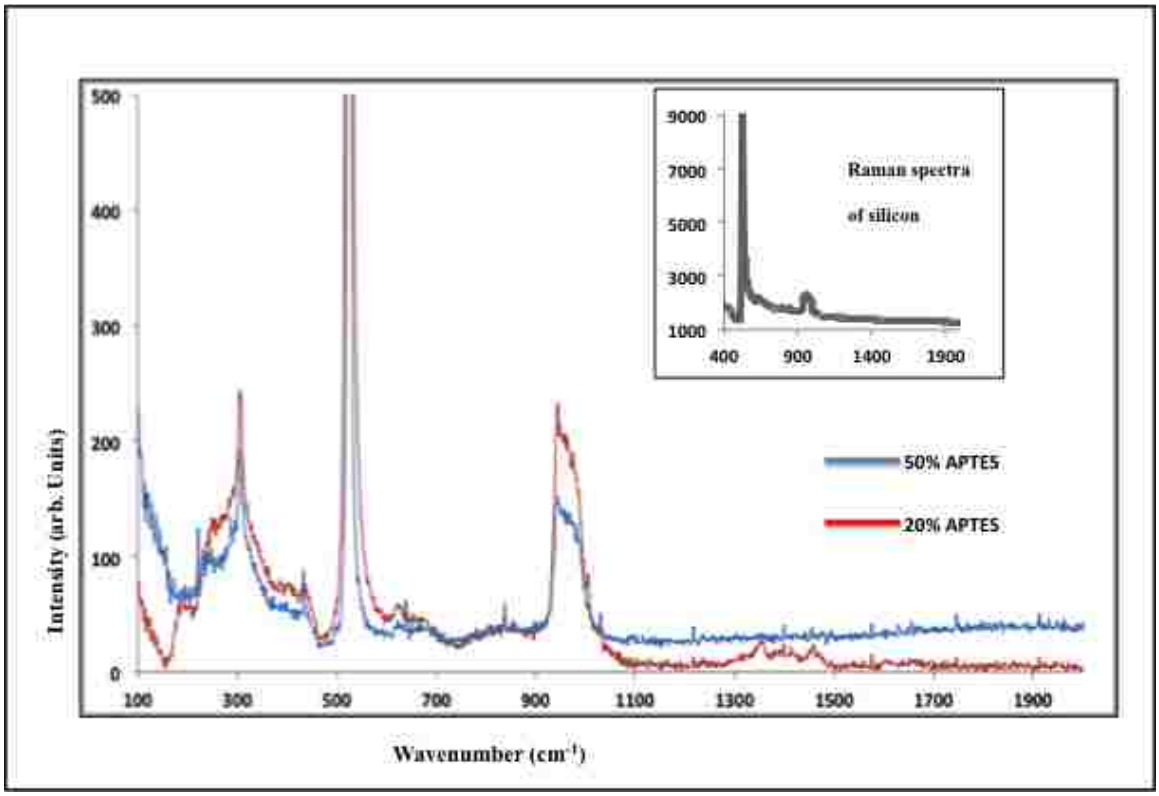

Figure 22: Shows Raman spectroscopy measurements of 50% and 20% APTES on silicon substrate. Inset shows Raman results of bare silicon sample.

4.5 Conclusions

APTES is widely used in organo-silane coupling agents for sensors. APTES is also used to bond organic probe molecules to silica sol-gel and glass substrates. Organo-silane coupling agents are useful for fiber optic sensor applications [7]. Gnyba et al. discusses the usage of organically modified silanes (ORMOSILs) in photonics to manufacture planar waveguides, Bragg gratings, lenses, and components for integrated optics. They also mention that the future applications of these materials may also include optical fiber sensors, biosensors, and solid state lasers. In conjunction with the characterization work of this thesis, APTES, due to its excellent bonding ability, was used as a binding agent to deposit CNTs on silicon substrates using the process of EPD.

From AFM measurements it was found that the average height (roughness) of the APTES molecules are found to be approximately 360 and 230nm for 50% and 20% concentrations, respectively. The diameters of the molecules are approximately 0.5 um. Raman spectra were obtained, and the positions of the peaks were analyzed. The peaks at 940 cm^{-1} are due to C-C skeletal vibrations. The 520 cm^{-1} peaks correspond to Si-O-Si network vibrations. As described, for this material N-H bond stretching is expected at 3310-3370 cm^{-1}.

5. CHARACTERIZATION OF ZEIN FIBERS

5.1 Introduction to Zein Fibers

In recent years, much attention has been given to addressing the various mechanical and chemical properties of biodegradable biopolymers. These polymers have barrier properties which are useful in the packaging industry due to their selective permeability. Biopolymers also possess properties that are suitable for increasing the shelf-life of a material. Bioplastics are used for packing in-flight catering products, packaging dairy products, and pesticide soil pins. Cellulose, starch, peptides, proteins, RNA, DNA, and chitin are examples of commonly used biopolymers.

Currently, a great deal of progress has been made in the development of biodegradable polymer blends and composites from starch, corn gluten meal, wheat gluten, and zein [66-67]. Zein is a class of biopolymer which falls into the category of prolamine proteins of corn (maize). The extraction of zein from corn protein meal using alcohol was first patented by Osborne [68]. It is a biodegradable material which is insoluble in water except in the presence of alcohol, high concentrations of urea, and high concentrations of alkali (pH 11 or above). Based on solubility and structures, zein can be classified into α, β, γ, and δ [69]. Composites of zein have unique characteristics and functionalities, and because of this they are used in various applications. Some of the important characteristics of zein composites include their high tensile strength, resistance to grease and water penetration, permeability, and non-allergic reactivity. Zein biopolymers are also used in fibers, films, plastics, coatings, adhesives, and ink. Since zein fibers are resistant to microbial attacks, it is commonly used in the pharmaceutical industries to coat capsules [34b]. Due to its selective permeability, it is also used to mask flavors and aromas [32]. When treated with formaldehyde, it has the ability to form an

essentially inert product [70]. Though numerous studies have addressed the mechanical and chemical properties of zein composites, to our knowledge little literature exists that addresses the potential for conductivity in zein composites. The conductive properties of zein fibers can potentially have numerous applications in the electronics industry.

In this study, we present some preliminary results addressing the properties of zein fibers by depositing them on various commonly used substrates such as aluminum (conductor) and glass (insulator). The zein fibers are deposited onto the substrates using an electrospinning technique. Atomic force microscopy (AFM) is used to characterize the surface morphology of the zein fibers on these different substrates.

5.2 Electrospinning Technique and Sample Preparation

We have used electrospinning to deposit zein composites on different substrates. The electrospinning process is an efficient one because of its ability to produce uniform fibers in the nanometer and micrometer ranges. Electrospinning is used in numerous fields such as: biotechnology, environmental engineering, tissue engineering, pharmaceutics, defense, and security[71].

The electrospinning process uses electrostatic forces to produce fine fibers; a DC voltage of order of 5-50 kV is used in this process. The laboratory set up for electrospinning consists of a spinneret, a high voltage power supply and a ground collector as shown in Figure 23. A melt (charged polymer solution) is fed through a nozzle or small opening. Because of the charge the solution is deposited as a jet onto a ground collector plate. When a sufficiently high voltage is applied to the liquid droplet leaving the nozzle, it gets charged, and stretched droplets emerge at a critical point. This point is known as the Taylor cone.

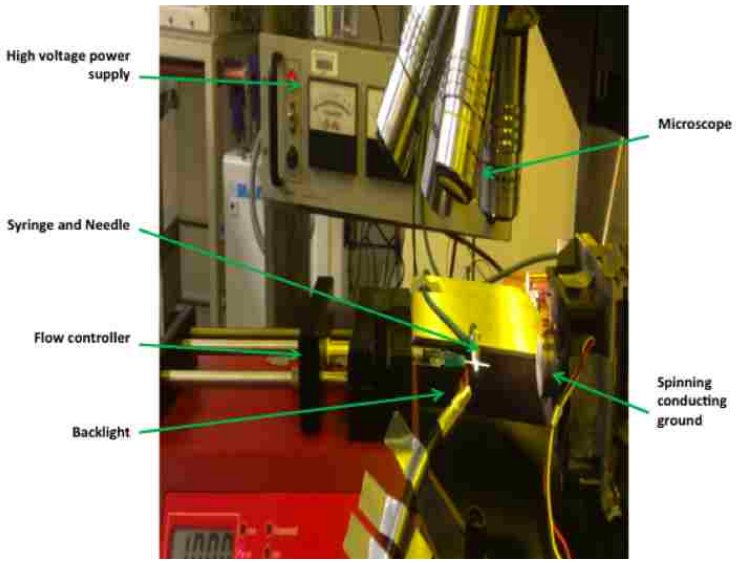

Figure 23: Electrospinning laboratory setup

The ground collector can be a metal plate, screen, or rotating mandrel. The schematic diagram of the electrospinning technique is in shown in Figure 24.

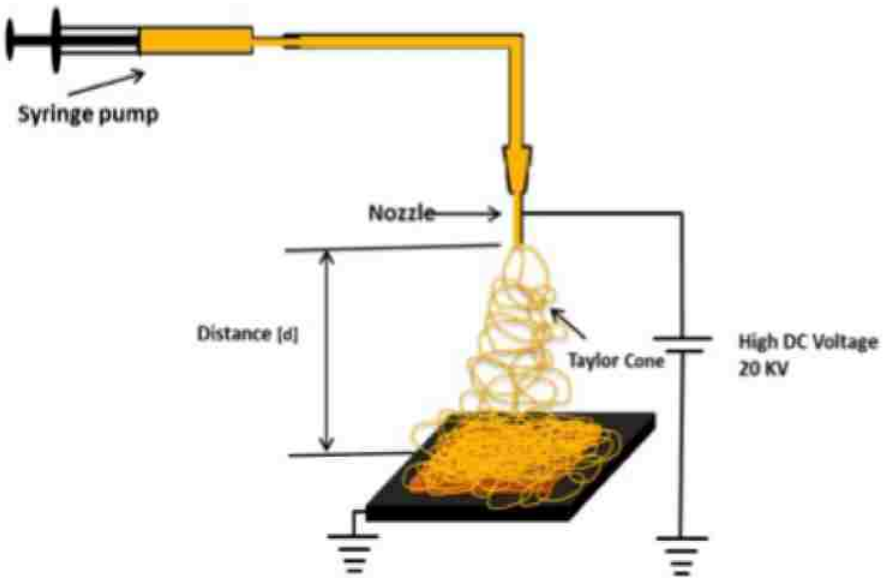

Figure 24: Schematic diagram of electrospinning technique

To produce zein fibers, we have used 0.1mg of zein combined with 0.264 ml of ethanol and 0.066 ml of DI water. This combination is agitated using an ultra-sonic bath for 10 minutes. Then the solution is allowed to stabilize overnight.

The morphology of electrospun zein fibers was examined using SEM. As discussed in section 2.6, SEM uses a focused electron beam to generate signals on the sample surface. Electron-sample interactions give information pertaining to morphology, chemical composition, and crystalline structure of the sample. Figure 25 shows SEM images of zein fibers.

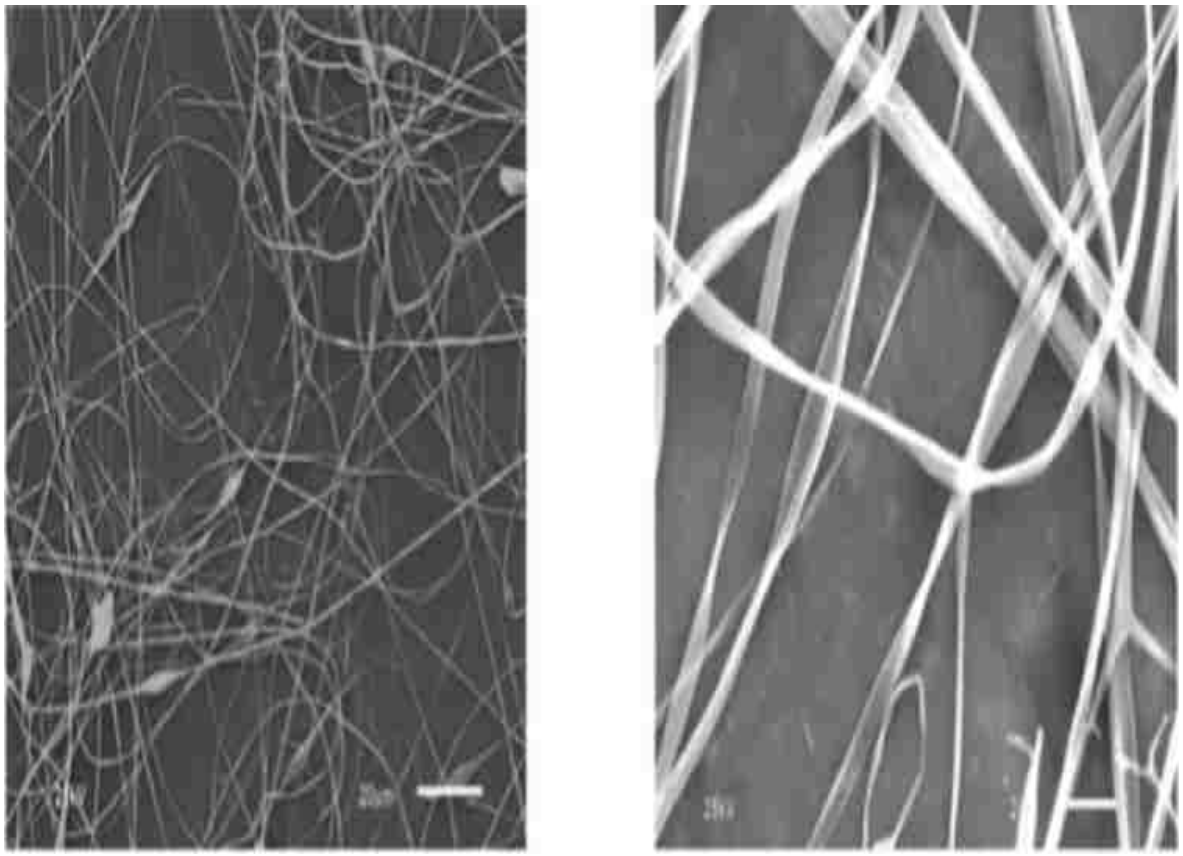

Figure 25: SEM images of electrospun zein fibers

Fibers deposited on different substrates were collected in bevel sample holders and were sputtered with Pd/Au under vacuum. To obtain SEM images, a high performance JSM-6610LV SEM apparatus with an accelerating voltage ranging from 300V to 30kV was used. Magnification of this instrument can be varied from 5x to 400,000x, with a resolution of 3.0nm at 30KV. SEM images of zein ultra fine fibers show ribbon like morphology mixed with a cylindrical shape.

5.3 Characterization of Zein Fibers Using AFM

5.3.1 Zein deposited on aluminum substrates

AFM images were obtained using contact mode. Experiments were performed using a 450 μm long and 50 μm wide silicon cantilever with aluminum detector coating, with a stiffness 0.18N/m, and with a cone angle of 40^0. The force applied by the probe varied between 0.06 to 0.14 N/m, depending on the type of material deposited on the substrate. Here, the topography of the sample is obtained when the tip follows trajectories of constant force derivatives. Figure 25 (a) and 25 (c) show zein fibers in a 35.75 x 35.75 μm^2 area and their corresponding line profiles in Figure 25 (b) and 25 (d). The images represent clustering of zein fibers. Using the Pacific Nanotechnology software, the average roughness of this area was found to be 79 nm. Figure 25(c) and (d) represent a zoomed in image of Fig. 25(a) and 25 (b) highlighting a typical zein fiber deposited on to the Al substrate. The average thickness and length of zein fibers were estimated to be approximately 1.4 μm and 4 μm, respectively.

5.3.2 Zein fibers deposited on glass substrates

Zein fibers were deposited on glass substrates and scanned using contact mode. Figure 26 (a) and (b) represent clustering of zein fibers in an 18.51 μm^2 area and their corresponding line profiles. Figure 26 (c) and (d) represent a zoomed-in image of 26(a) and its corresponding line profile. The average thickness and length of zein fibers deposited on glass substrate were found to be approximately1.3 μm and 7μm.

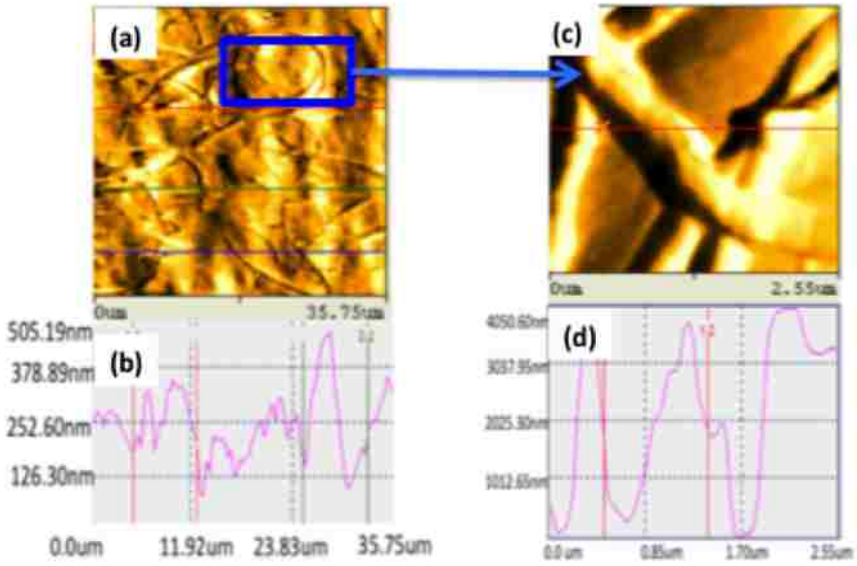

Figure 26:AFM images of zein fibers on aluminum substrate (a) 35.75 x 35.75 um^2 area (c) 2.55x2.55 um^2 area. (b) and (d) represent line profiles of (a) and (b).

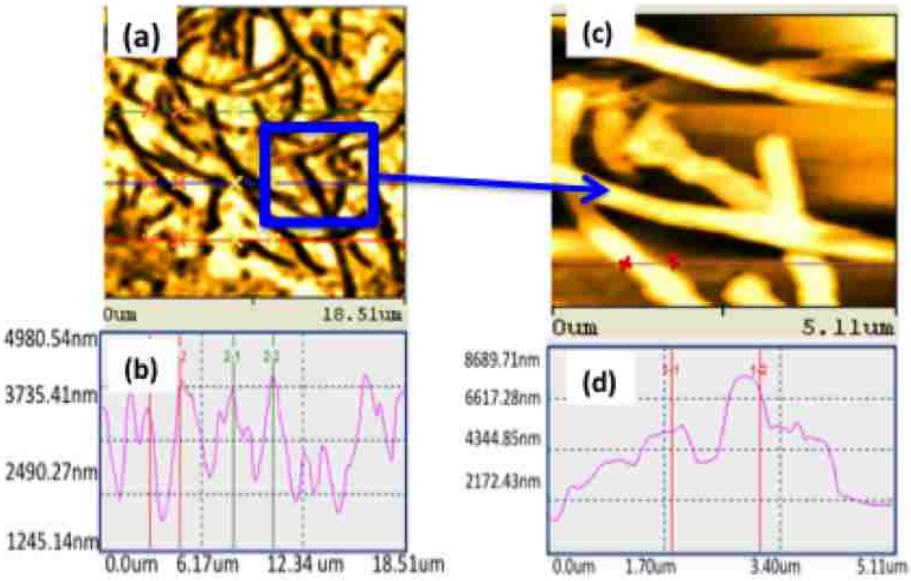

Figure 27:AFM images of zein fibers on aluminum substrate (a) 18.51 x 18.51 um^2 area (b) 5.11 x 5.11 um^2 area. (c) and (d) represent line profiles of (a) and (b).

5.4 Raman spectroscopy Analysis of Zein Fibers

Zein fibers were deposited on aluminum and glass substrates and examined using Raman spectroscopy. For measurements, a HeNe laser with a wavelength of 638.4 nm and an incident power of 17 mW was used. The confocal hole aperture of 200 μm and grating of 1800 lines per mm were selected in the Jobin Yvon Horiba Labram Raman spectrometer used for this study. Scans were performed in the 100 and 3100 cm^{-1} range using a 100x objective. The bands at 1447 and 1450 cm^{-1} on glass and aluminum substrates correspond to CH_3 anti-symmetric deformation [72]. The intensity at wavenumber 1649 and 1652 cm^{-1} (Al and glass) correspond to the symmetric carbonyl (C=O) stretch [72]. Wavenumbers 2874 and 2867 cm^{-1} (Al and glass) represent the CH_3 and CH_2 antisymmetric stretch, respectively. The broad peak at 2930 and 2899 cm^{-1} (Al and glass) reflects the presence of water in the mixture and originates from an -OH group [72]. Raman spectroscopy measurements of zein fibers are shown in the Figure 27.

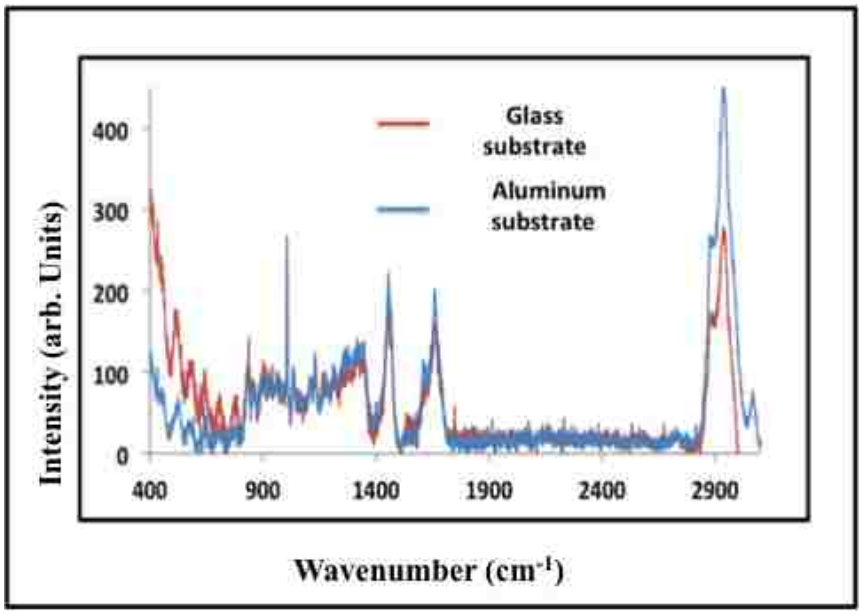

Figure 28: Raman spectroscopy measurements of zein fibers deposited on two different substrates

5.5 Conclusions

Zein fibers were deposited on Al and glass substrates using an electrospinning technique, and these fibers were characterized using SEM, AFM, and Raman spectroscopy. The images obtained using SEM are shown in section 5.4. AFM images on the Al substrate depict that the average thickness and length of the fibers are approximately 1.4 μm and 4 μm, respectively. AFM images obtained on the glass substrate indicate that the average thickness and length of fibers are approximately 1.3 μm and 7 μm, respectively. Raman spectroscopy results were obtained and the position of each peak was analyzed.

Recommendations for future work include a detailed characterization of zein and CNT composites using AFM, SEM, and Raman spectroscopy. Because, CNTs exhibit conductivity, it is possible that zein-CNT composites may have good electrical properties. As such, CP-AFM can be used to obtain I-V characteristics of zein CNT composites.

6. CONCLUSIONS AND FUTURE WORK

In this work we have characterized different HEMs using AFM, CP-AFM, and Raman spectroscopy techniques with supportive imaging via SEM for certain samples. Using AFM, dimensions of molecules and fibers have been obtained. The CP-AFM technique was used to determine I-V characteristics of [R6G][TPB] GUMBOS. Vibrational states of molecules and various peaks are analyzed using Raman spectroscopy.

Atomic Force Microscopy and conductive probe AFM experiments were successfully performed on a new class of materials known as GUMBOS. With AFM images, the diameter of each [R6G][TPB] molecule was found to be between 200-500nm, and the current values obtained from CP-AFM measurements were approximately between 10^{-6} to 10^{-7} A, for a voltage range of 0 to 1 V. The resistance value was found to be in the 0.3 to 3 MΩ range. The main advantage of using GUMBOS in electronic applications is the ease of synthesis of nanoparticles from parent compounds, and also, by varying the anionic or cationic components in their structure, high thermal stability and adaptable functionality can be achieved.

APTES molecules were studied using AFM and Raman spectroscopy techniques. From AFM measurements, the typical diameter of a molecule was found to be approximately 0.5 μm. Raman spectra were obtained, and the positions of peaks were analyzed. The bands at 940 cm^{-1} are due to C-C skeletal vibrations. The peak at 520 cm^{-1} corresponds to Si-O-Si network vibrations. N-H bond stretching is expected at 3310-3370 cm^{-1}. Related work indicates that APTES may be used as a binding agent to deposit CNTs on silicon substrates using the process of electrophoretic deposition (EPD).

Zein fibers are biodegradable polymers that are used extensively in the food and drug industry. In this study, we present some preliminary results addressing the properties of zein

composites by depositing them on various commonly used substrates such as aluminum (conductor) and glass (insulator) using an electrospinning technique. These fibers were characterized using SEM, AFM, and Raman spectroscopy. The average thickness and length of zein fibers deposited onto Al were estimated to be approximately 1.4 μm and 4 μm, respectively, and the average thickness and length of zein fibers deposited on glass were found to be approximately1.3 μm and 7 μm, respectively. Raman spectroscopy results were obtained, and the position of each peak was analyzed.

Recommendations for future work include additional characterization of zein and CNT composites using AFM, SEM, and Raman spectroscopy with variations in the techniques of and conditions for synthesis and deposition. In particular, since CNTs exhibit conductivity, it is possible that zein-CNT composites may also have good electrical properties. As such, CP-AFM can be used to obtain the I-V characteristics of these hybrid electronic materials.

REFERENCES

1. Zhang, L.; Webster, T. J., Nanotechnology and nanomaterials: promises for improved tissue regeneration. *Nano Today* **2009,** *4* (1), 66-80.

2. (a) Chang, K., Oldest Bacteria Fossils? Or Are They Merely Tiny Rock Flaws? *New York Times* Mar 12, 2002, p F4; (b) Feynman, R. P.,
There's Plenty of Room at the Bottom–An Invitation to Enter a New Field of Physics, 1959. *Adres:* http://www. *zyvex. com/nanotech/feynman. html* **2010**.

3. Daniels-Race, T., 2014.

4. C.Binns, *Introduction to nanoscience and nanotechnology* 2010.

5. Judeinstein, P.; Sanchez, C., Hybrid organic–inorganic materials: a land of multidisciplinarity. *J. Mater. Chem.* **1996,** *6* (4), 511-525.

6. Ogoshi, T.; Chujo, Y., Organic–inorganic polymer hybrids prepared by the sol-gel method. *Composite Interfaces* **2005,** *11* (8-9), 539-566.

7. Nivens, D. A.; Zhang, Y.; Angel, S. M., A fiber-optic pH sensor prepared using a base-catalyzed organo-silica sol–gel. *Analytica chimica acta* **1998,** *376* (2), 235-245.

8. Weimer, R.; Lenahan, P.; Marchione, T.; Brinker, C., Electronic properties of sol-gel-derived oxides on silicon. *Applied physics letters* **1987,** *51* (15), 1179-1181.

9. Warren, W.; Lenahan, P.; Brinker, C.; Ashley, C.; Reed, S.; Shaffer, G., Sol-gel silicate thin-film electronic properties. *Journal of Applied Physics* **1991,** *69* (8), 4404-4408.

10. Banger, K.; Yamashita, Y.; Mori, K.; Peterson, R.; Leedham, T.; Rickard, J.; Sirringhaus, H., Low-temperature, high-performance solution-processed metal oxide thin-film transistors formed by a 'sol–gel on chip'process. *Nature materials* **2010,** *10* (1), 45-50.

11. Ma, Z.; Yu, J.; Dai, S., Preparation of inorganic materials using ionic liquids. *Advanced Materials* **2010,** *22* (2), 261-285.

12. Dai, S.; Ju, Y.; Gao, H.; Lin, J.; Pennycook, S.; Barnes, C., Preparation of silica aerogel using ionic liquids as solvents. *Chem. Commun.* **2000,** (3), 243-244.

13. Nakashima, T.; Kimizuka, N., Interfacial synthesis of hollow TiO2 microspheres in ionic liquids. *Journal of the American Chemical Society* **2003,** *125* (21), 6386-6387.

14. Zhou, Y.; Antonietti, M., Synthesis of very small TiO2 nanocrystals in a room-temperature ionic liquid and their self-assembly toward mesoporous spherical aggregates. *Journal of the American Chemical Society* **2003,** *125* (49), 14960-14961.

15. (a) Kim, K.-S.; Demberelnyamba, D.; Lee, H., Size-selective synthesis of gold and platinum nanoparticles using novel thiol-functionalized ionic liquids. *Langmuir* **2004,** *20* (3), 556-560; (b) Kim, K.-S.; Demberelnyamba, N. D.; Yeon, S.-W.; Choi, S.; Cha, J.-H.; Lee, H., One-phase preparation of palladium nanoparticles using thiol-functionalized ionic liquid. *Korean Journal of Chemical Engineering* **2005,** *22* (5), 717-720.

16. Tesfai, A.; El-Zahab, B.; Bwambok, D. K.; Baker, G. A.; Fakayode, S. O.; Lowry, M.; Warner, I. M., Controllable formation of ionic liquid micro-and nanoparticles via a melt–emulsion–quench approach. *Nano letters* **2008,** *8* (3), 897-901.

17. Bwambok, D. K.; El-Zahab, B.; Challa, S. K.; Li, M.; Chandler, L.; Baker, G. A.; Warner, I. M., Near-infrared fluorescent nanoGUMBOS for biomedical imaging. *ACS nano* **2009,** *3* (12), 3854-3860.

18. Tesfai, A.; El-Zahab, B.; Kelley, A. T.; Li, M.; Garno, J. C.; Baker, G. A.; Warner, I. M., Magnetic and nonmagnetic nanoparticles from a group of uniform materials based on organic salts. *ACS nano* **2009,** *3* (10), 3244-3250.

19. Huddleston, J.; Rogers, R., Room temperature ionic liquids as novel media for 'clean'liquid–liquid extraction. *Chemical Communications* **1998,** (16), 1765-1766.

20. áde Rooy, S. L., Fluorescent one-dimensional nanostructures from a group of uniform materials based on organic salts. *Chemical Communications* **2011,** *47* (31), 8916-8918.

21. Das, S.; Bwambok, D.; El-Zahab, B.; Monk, J.; de Rooy, S. L.; Challa, S.; Li, M.; Hung, F. R.; Baker, G. A.; Warner, I. M., Nontemplated approach to tuning the spectral properties of cyanine-based fluorescent NanoGUMBOS. *Langmuir* **2010,** *26* (15), 12867-12876.

22. Lu, C.; Das, S.; Magut, P. K.; Li, M.; El-Zahab, B.; Warner, I. M., Irradiation Induced Fluorescence Enhancement in PEGylated Cyanine-Based NIR Nano-and Mesoscale GUMBOS. *Langmuir* **2012,** *28* (40), 14415-14423.

23. Cole, M. R.; Li, M.; Jadeja, R.; El-Zahab, B.; Hayes, D.; Hobden, J. A.; Janes, M. E.; Warner, I. M., Minimizing human infection from Escherichia coli O157: H7 using GUMBOS. *Journal of Antimicrobial Chemotherapy* **2013,** *68* (6), 1312-1318.

24. Ruiz-Hitzky, E.; Darder, M.; Aranda, P.; Ariga, K., Advances in biomimetic and nanostructured biohybrid materials. *Advanced Materials* **2010,** *22* (3), 323-336.

25. Zhang, Q.; Ariga, K.; Okabe, A.; Aida, T., A condensable amphiphile with a cleavable tail as a "lizard" template for the sol-gel synthesis of functionalized mesoporous silica. *Journal of the American Chemical Society* **2004,** *126* (4), 988-989.

26. Lee, J.; Kim, J.; Kim, J.; Jia, H.; Kim, M. I.; Kwak, J. H.; Jin, S.; Dohnalkova, A.; Park, H. G.; Chang, H. N., Simple synthesis of hierarchically ordered mesocellular mesoporous silica materials hosting crosslinked enzyme aggregates. *Small* **2005,** *1* (7), 744-753.

27. Böttcher, H.; Soltmann, U.; Mertig, M.; Pompe, W., Biocers: ceramics with incorporated microorganisms for biocatalytic, biosorptive and functional materials development. *Journal of Materials Chemistry* **2004,** *14* (14), 2176-2188.

28. Zhao, X.; Mai, Z.; Kang, X.; Zou, X., Direct electrochemistry and electrocatalysis of horseradish peroxidase based on clay–chitosan-gold nanoparticle nanocomposite. *Biosensors and Bioelectronics* **2008,** *23* (7), 1032-1038.

29. Darder, M.; Aranda, P.; Ruiz-Hitzky, E., Bionanocomposites: a new concept of ecological, bioinspired, and functional hybrid materials. *Advanced Materials* **2007,** *19* (10), 1309-1319.

30. Szabó, T.; Mitea, R.; Leeman, H.; Premachandra, G. S.; Johnston, C. T.; Szekeres, M.; Dékány, I.; Schoonheydt, R. A., Adsorption of protamine and papain proteins on saponite. *Clays and Clay Minerals* **2008,** *56* (5), 494-504.

31. Forano, C.; Vial, S.; Mousty, C., Nanohybrid enzymes-layered double hydroxides: potential applications. *Current Nanoscience* **2006,** *2* (3), 283-294.

32. Shukla, R.; Cheryan, M., Zein: the industrial protein from corn. *Industrial Crops and Products* **2001,** *13* (3), 171-192.

33. Croston, C. B.; Evans, C.; Smith, A., Zein Fibers. *Industrial & engineering chemistry* **1945,** *37* (12), 1194-1198.

34. (a) Sozer, N.; Kokini, J. L., Nanotechnology and its applications in the food sector. *Trends in biotechnology* **2009,** *27* (2), 82-89; (b) Torres-Giner, S.; Gimenez, E.; Lagarón, J. M., Characterization of the morphology and thermal properties of zein prolamine nanostructures obtained by electrospinning. *Food Hydrocolloids* **2008,** *22* (4), 601-614; (c) Shi, K.; Kokini, J. L.; Huang, Q., Engineering zein films with controlled surface morphology and hydrophilicity. *Journal of agricultural and food chemistry* **2009,** *57* (6), 2186-2192.

35. Lai, H. M.; Geil, P.; Padua, G., X-ray diffraction characterization of the structure of zein–Oleic acid films. *Journal of applied polymer science* **1999,** *71* (8), 1267-1281.
36. Lange, D.; Hagleitner, C.; Hierlemann, A.; Brand, O.; Baltes, H., Complementary metal oxide semiconductor cantilever arrays on a single chip: mass-sensitive detection of volatile organic compounds. *Analytical Chemistry* **2002,** *74* (13), 3084-3095.

37. (a) Binnig, G.; Rohrer, H., Scanning tunneling microscopy-from birth to adolescence. *Physics 1981-1990* **1993,** *2*, 389; (b) Giessibl, F. J., Advances in atomic force microscopy. *Reviews of modern physics* **2003,** *75* (3), 949.

38. Meyer, E., Atomic force microscopy. *Progress in surface science* **1992,** *41* (1), 3-49.

39. Grothe, B.; Park, T., Structure and function of the bat superior olivary complex. *Microscopy Research and Technique* **2000,** *51* (4), 382-402.

40. Moss, C. F.; Sinha, S. R., Neurobiology of echolocation in bats. *Current Opinion in Neurobiology* **2003,** *13* (6), 751-758.

41. DeLong, C. M.; Bragg, R.; Simmons, J. A., Evidence for spatial representation of object shape by echolocating bats (Eptesicus fuscus). *Journal of the Acoustical Society of America* **2008,** *123* (6), 4582-4598.

42. Avila-Flores, R.; Medellin, R. A., Ecological, taxonomic, and physiological correlates of cave use by mexican bats. *Journal of Mammalogy* **2004,** *85* (4), 675-687.

43. Paulo, Á.; García, R., Tip-surface forces, amplitude, and energy dissipation in amplitude-modulation (tapping mode) force microscopy. *Physical Review B* **2001,** *64* (19).

44. Eurobats Secretariat Eurobats: The Agreement on the Conservation of Populations of European Bats. http://www.eurobats.org/index.htm (accessed April 1).

45. Dufrene, Y. F., Atomic Force Microscopy, a Powerful Tool in Microbiology. *Journal of Bacteriology* **2002,** *184* (19), 5205-5213.

46. Solares, S. D., Frequency and force modulation atomic force microscopy: low-impact tapping-mode imaging without bistability. *Measurement Science and Technology* **2007,** *18* (7), L9-L14.

47. Skårman, B.; Wallenberg, L. R.; Jacobsen, S. N.; Helmersson, U.; Thelander, C., Evaluation of intermittent contact mode AFM probes by HREM and using atomically sharp CeO2 ridges as tip characterizer. *Langmuir* **2000,** *16* (15), 6267-6277.

48. (a) Montelius, L.; Tegenfeldt, J., Direct observation of the tip shape in scanning probe microscopy. *Applied physics letters* **1993,** *62* (21), 2628-2630; (b) Montelius, L.; Tegenfeldt, J.; Van Heeren, P., Direct observation of the atomic force microscopy tip using inverse atomic force microscopy imaging. *Journal of Vacuum Science & Technology B* **1994,** *12* (3), 2222-2226.

49. Solares, S. D., Eliminating bistability and reducing sample damage through frequency and amplitude modulation in tapping-mode atomic force microscopy. *Measurement Science and Technology* **2007,** *18* (3), 592.

50. Laboratory of photo induced effects vibrational and X-ray spectroscopies. http://www.fis.unipr.it/phevix/raman_tutorial.html.

51. Raman Spectroscopy Basics. http://content.piacton.com/Uploads/Princeton/Documents/Library/UpdatedLibrary/Raman_Spectroscopy_Basics.pdf.

52. Borjesson, J., SEM. **2006**.

53. Cole, M. Chemical and Biological Evaluation of Antibiotic-based Ionic Liquids and GUMBOS Against Pathogenic Bacteria. Faculty of the Louisiana State University and Agricultural and Mechanical College in partial fulfillment of the requirements for the degree of Doctor of Philosophy in The Department of Chemistry by Marsha Cole BS, Grambling State University, 2012.

54. Sarkar, A.; Kanakamedala, K.; Rajathadripura, M. D.; Jagadish, N. N.; Magut, P. K.; de Rooy, S.; Das, S.; El-Zahab, B.; Warner, I. M.; Daniels-Race, T., Electro-optical characterization of nanoGUMBOS.

55. Sarkar, A.; Kanakamedala, K.; Jagadish, N. N.; Daniels-Race, T.; Jordan, A.; Das, S.; Siraj, N.; Warner, I. M., Electro-optical characterization of cyanine-based GUMBOS and nanoGUMBOS.

56. Lyubchenko, Y. L.; Oden, P. I.; Lampner, D.; Lindsay, S. M.; Dunker, K. A., Atomic force microscopy of DNA and bacteriophage in air, water and propanol: the role of adhesion forces. *Nucleic Acids Research* **1993,** *21* (5), 1117-1123.

57. Karrasch, S.; Dolder, M.; Schabert, F.; Ramsden, J.; Engel, A., Covalent binding of biological samples to solid supports for scanning probe microscopy in buffer solution. *Biophysical journal* **1993,** *65* (6), 2437-2446.

58. Vandenberg, E. T.; Bertilsson, L.; Liedberg, B.; Uvdal, K.; Erlandsson, R.; Elwing, H.; Lundström, I., Structure of 3-aminopropyl triethoxy silane on silicon oxide. *Journal of Colloid and Interface Science* **1991,** *147* (1), 103-118.

59. Sarkar, A.; Daniels-Race, T., Electrophoretic Deposition of Carbon Nanotubes on 3-Amino-Propyl-Triethoxysilane (APTES) Surface Functionalized Silicon Substrates. *Nanomaterials* **2013,** *3* (2), 272-288.

60. Howarter, J. A.; Youngblood, J. P., Optimization of silica silanization by 3-aminopropyltriethoxysilane. *Langmuir* **2006,** *22* (26), 11142-11147.

61. Sarkar, A. Electrophoretic Deposition of Carbon Nanotubes on Silicon Substrates. Louisiana State University, 2013.

62. Pézolet, M.; Pigeon, M.; Menard, D.; Caille, J., Raman spectroscopy of cytoplasmic muscle fiber proteins. Orientational order. *Biophysical journal* **1988,** *53* (3), 319-325.

63. Spizzirri, P.; Fang, J.-H.; Rubanov, S.; Gauja, E.; Prawer, S., Nano-Raman spectroscopy of silicon surfaces. *arXiv preprint arXiv:1002.2692* **2010**.

64. Gnyba, M.; Keränen, M.; Kozanecki, M.; Kosmowski, B. B., Raman investigation of hybrid polymer thin films. *Materials Science (0137-1339)* **2005,** *23* (1).

65. Lin-Vien, D.; Colthup, N. B.; Fateley, W. G.; Grasselli, J. G., *The handbook of infrared and Raman characteristic frequencies of organic molecules*. Elsevier: 1991.

66. (a) Gaspar, M.; Benkő, Z.; Dogossy, G.; Reczey, K.; Czigany, T., Reducing water absorption in compostable starch-based plastics. *Polymer Degradation and Stability* **2005,** *90* (3), 563-569; (b) Grazuleviciene, V.; Augulis, L.; Grazulevicius, J.; Kapitanovas, P.; Vedegyte, J., Biodegradable starch, PVA, and peat composites for agricultural use. *Russian Journal of Applied Chemistry* **2007,** *80* (11), 1928-1930.

67. Kim, S.; Xu, J.; Liu, S., Production of biopolymer composites by particle bonding. *Composites Part A: Applied Science and Manufacturing* **2010,** *41* (1), 146-153.

68. Osborne, T. B., Process of extracting zein. Google Patents: 1891.

69. Coleman, C. E.; Larkins, B. A., The prolamins of maize. In *seed Proteins*, Springer: 1999; pp 109-139.

70. Lawton, J. W., Zein: A history of processing and use. *Cereal Chemistry* **2002,** *79* (1), 1-18.

71. Bhardwaj, N.; Kundu, S. C., Electrospinning: a fascinating fiber fabrication technique. *Biotechnology advances* **2010,** *28* (3), 325-347.

72. Oriero, D. A.; Weakley, A. T.; Aston, D. E., Rheological and micro-Raman time-series characterization of enzyme sol–gel solution toward morphological control of electrospun fibers. *Science and Technology of Advanced Materials* **2012,** *13* (2), 025008.

APPENDIX A: ADDITIONAL INFORMATION CONCERNING ZEIN FIBERS

Roughness analysis of zein fibers

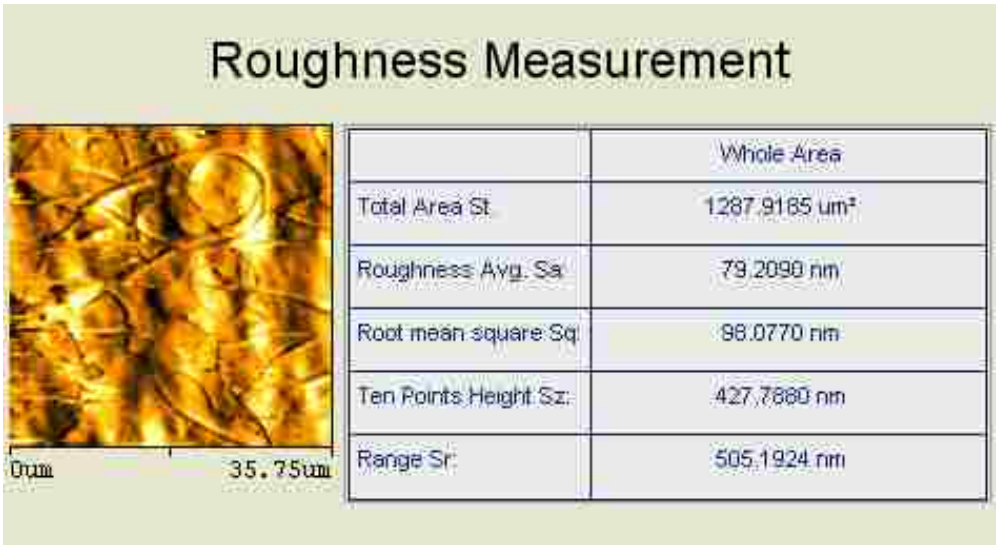

Figure 29:Roughness analysis of zein fibers on aluminum substrate (35.75X 35.75 um^2 area)

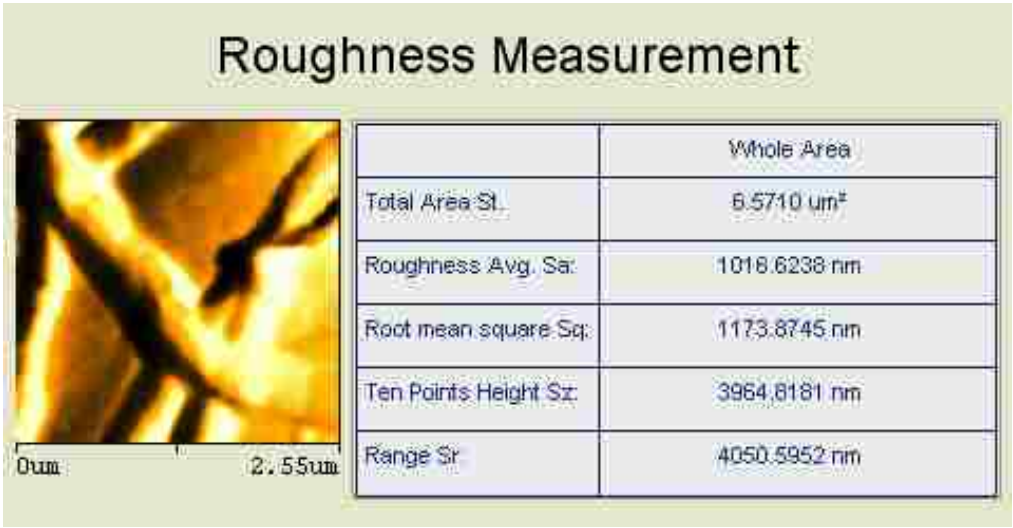

Figure 30: Roughness analysis of zein fibers on aluminum substrate (2.55X 2.55 um^2 area)

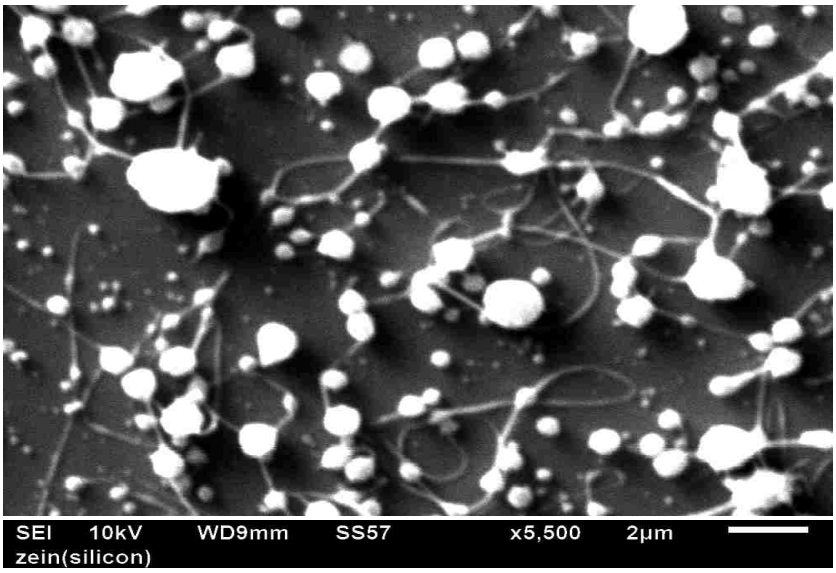

Figure 31:SEM image of zein fiber on silicon substrate

Figure 32:Roughness analysis of zein fibers on glass substrate (18.51X18.51 um^2 area)

Figure 33:Roughness analysis of zein fibers on glass substrate (5.11X5.11 um^2 area)

APPENDIX B: PERMISSIONS FOR USE OF COPYRIGHTED MATERIALS

Copyright Clearance Center RightsLink®

Home | Account Info | Help

ACS Publications

Title: Magnetic and Nonmagnetic Nanoparticles from a Group of Uniform Materials Based on Organic Salts

Author: Aaron Tesfai, Bilal El-Zahab, Algernon T. Kelley, Min Li, Jayne C. Garno, Gary A. Baker, and Isiah M. Warner

Publication: ACS Nano

Publisher: American Chemical Society

Date: Oct 1, 2009

Copyright © 2009, American Chemical Society

Logged in as: Madhavi Rajathadripura

LOGOUT

PERMISSION/LICENSE IS GRANTED FOR YOUR ORDER AT NO CHARGE

This type of permission/license, instead of the standard Terms & Conditions, is sent to you because no fee is being charged for your order. Please note the following:

- Permission is granted for your request in both print and electronic formats, and translations.
- If figures and/or tables were requested, they may be adapted or used in part.
- Please print this page for your records and send a copy of it to your publisher/graduate school.
- Appropriate credit for the requested material should be given as follows: "Reprinted (adapted) with permission from (COMPLETE REFERENCE CITATION). Copyright (YEAR) American Chemical Society." Insert appropriate information in place of the capitalized words.
- One-time permission is granted only for the use specified in your request. No additional uses are granted (such as derivative works or other editions). For any other uses, please submit a new request.

If credit is given to another source for the material you requested, permission must be obtained from that source.

BACK CLOSE WINDOW

Home | Account Info | Help

Title: Controllable Formation of Ionic Liquid Micro- and Nanoparticles via a Melt–Emulsion–Quench Approach

Author: Aaron Tesfai, Bilal El-Zahab, David K. Bwambok, Gary A. Baker, Sayo O. Fakayode, Mark Lowry, and Isiah M. Warner

Publication: Nano Letters

Publisher: American Chemical Society

Date: Mar 1, 2008

Logged in as:
Madhavi Rajathadripura

LOGOUT

PERMISSION/LICENSE IS GRANTED FOR YOUR ORDER AT NO CHARGE

This type of permission/license, instead of the standard Terms & Conditions, is sent to you because no fee is being charged for your order. Please note the following:

- Permission is granted for your request in both print and electronic formats, and translations.
- If figures and/or tables were requested, they may be adapted or used in part.
- Please print this page for your records and send a copy of it to your publisher/graduate school.
- Appropriate credit for the requested material should be given as follows: "Reprinted (adapted) with permission from (COMPLETE REFERENCE CITATION). Copyright (YEAR) American Chemical Society." Insert appropriate information in place of the capitalized words.
- One-time permission is granted only for the use specified in your request. No additional uses are granted (such as derivative works or other editions). For any other uses, please submit a new request.

If credit is given to another source for the material you requested, permission must be obtained from that source.

BACK | CLOSE WINDOW

ROYAL SOCIETY OF CHEMISTRY LICENSE TERMS AND CONDITIONS

Jun 14, 2014

This is a License Agreement between Madhavi Rajathadripura ("You") and Royal Society of Chemistry ("Royal Society of Chemistry") provided by Copyright Clearance Center ("CCC"). The license consists of your order details, the terms and conditions provided by Royal Society of Chemistry, and the payment terms and conditions.

All payments must be made in full to CCC. For payment instructions, please see information listed at the bottom of this form.

License Number	3407450229919
License date	Jun 14, 2014
Licensed content publisher	Royal Society of Chemistry
Licensed content publication	Chemical Communications (Cambridge)
Licensed content title	Fluorescent one-dimensional nanostructures from a group of uniform materials based on organic salts
Licensed content author	Sergio L. de Rooy,Bilal El-Zahab,Min Li,Susmita Das,Ellen Broering,Lin Chandler,Isiah M. Warner
Licensed content date	Jun 15, 2011
Volume number	47
Issue number	31
Type of Use	Thesis/Dissertation
Requestor type	academic/educational
Portion	figures/tables/images
Number of figures/tables /images	1
Format	electronic
Distribution quantity	1
Will you be translating?	no
Order reference number	None
Title of the thesis/dissertation	Characterization of Hybrid Electronic Materials Using Atomic Force Microscopy
Expected completion date	Aug 2014
Estimated size	100
Total	0.00 USD
Terms and Conditions	

PERMISSIONS REQUEST FORM FOR COPYRIGHT MATERIAL

To: **Dr.Isiah M. Warner**

From: **Madhavi D. Rajathadripura**[†], **Louisiana State University**, School of Electrical Engineering & Computer Science, Division of Electrical & Computer Engineering, Baton Rouge, LA 70803
phone: 225-572-6541; fax: (225) 578-5200; email: mrajat1@lsu.edu

I am preparing my MS thesis entitled *Characterization of Hybrid Electronic Materials Using Atomic Force Microscopy*. I request your permission to use a copy of the following figure:

Journal: Tesfai, A.; El-Zahab, B.; Bwambok, D. K.; Baker, G. A.; Fakayode, S. O.; Lowry, M.; Warner, I. M., Controllable formation of ionic liquid micro-and nanoparticles via a melt–emulsion–quench approach. *Nano letters* **2008,** *8* (3), 897-901.

Figure description: Scheme 1: Schematic showing the steps involved in the Melt-Emulsion-Quench Method for synthesizing Nano- and Microparticles using Surfactantless (Method 1) and surfactant-Assisted (Method 2) Procedures.

Journal : Tesfai, A.; El-Zahab, B.; Kelley, A. T.; Li, M.; Garno, J. C.; Baker, G. A.; Warner, I. M., Magnetic and nonmagnetic nanoparticles from a group of uniform materials based on organic salts. *ACS nano* **2009,** *3* (10), 3244-3250.

Figure description: Scheme 1: Basic processes for nanoparticle formation within AOT reverse micelles. Individual reverse micelles are shown without free surfactants (a) $[Bm_2Im][BF_4]$ nanoGUMBOS. (b) $[Bm_2Im][FeCl_4]$ magnetic GUMBOS particles.

Journal: de Rooy, S. L.; El-Zahab, B.; Li, M.; Das, S.; Broering, E.; Chandler, L.; Warner, I. M., Fluorescent one-dimensional nanostructures from a group of uniform materials based on organic salts. *Chemical Communications* **2011,** *47* (31), 8916-8918.

[†] **Major Professor**: Dr. Theda Daniels-Race, tdrace@lsu.edu, (225) 578-5623

Figure discription: Fig. 1: Chemical structure of [R6G][TPB].

Full acknowledgement will be given to the source of the material. Please indicate below if you require any special form of acknowledgement:

If you agree, please **sign below and either fax back (225-578-5200) or scan and send in email** (mrajat1@lsu.edu) to me.* In approving this request, you warrant that you are the sole owner of the rights granted (or are authorized to give permission for use of the aforementioned material) and that your material does not infringe anyone else's copyright. If you do not control these rights, please let me know who I should contact.

Permission is granted for use of the material cited:

Signed..... Date.....06/20/14.....

Thank you very much for your help. Please return the form to me at the address (email or fax) given above. *If you prefer, please let me know when/where, and I can pick up a hardcopy from your office.

Hi Anirban,

How are you doing and hows job? I am working on my thesis and I am writing about APTES characterization using AFM. So can I include following figure from your nanomaterials paper? Please let me know.

Figure 1. Schematic diagram displaying the process of hydroxylation after piranha treatment and silanization by 3-aminopropyl-triethoxysilane (APTES) treatment on silicon surface prior to the electrophoretic deposition (EPD) step.

Thanks**,**
Madhavi

Anirban <for.anirban@gmail.com> 14 June 2014
To: Madhavi Divakar Rajathadripura <mrajat1@lsu.edu>

Maddy,
You have my permission. But to bulletproof it, go ahead and seek copyright permission for using it from the journal.

Ty-Anirban

VITA

Madhavi Rajathadripura is from the city of Bengaluru, in India. She completed her Bachelor of Engineering degree in Electrical and Electronics Engineering from Visveswaraya Technological University in 2008. In Spring 2012, she enrolled as a graduate student in the department of Electrical and Computer Engineering at Louisiana State University. She is a candidate for the M.S. degree in Electrical and Computer Engineering to be awarded in Summer 2014. After graduation, she plans to work in industry.